IEEE Access
Multidisciplinary | Rapid Review | Open Access Journal

Received 29 November 2022, accepted 10 December 2022, date of publication 12 December 2022,
date of current version 19 December 2022.

Digital Object Identifier 10.1109/ACCESS.2022.3228828

RESEARCH ARTICLE

Modeling and Characterization of Traffic Flow Patterns and Identification of Airspace Density for UTM Application

ABDULRAHMAN ALHARBI, IVAN PETRUNIN, (Member, IEEE), AND DIMITRIOS PANAGIOTAKOPOULOS

School of Aerospace, Transport and Manufacturing (SATM), Cranfield University, MK43 0AL Bedford, U.K.

Corresponding author: Abdulrahman Alharbi (abdulrahman.a.alharbi@cranfield.ac.uk)

ABSTRACT Current airspace has limited resources, and the widespread use of unmanned aerial vehicles (UAVs) increases airspace density, which is already crowded with manned aircraft. This demands the improvement of airspace safety and capacity while considering all parametric uncertainties that may hinder aircraft and UAV mobility such as dynamic airspace structures and weather conditions. This paper proposes a data analytics framework to characterize traffic flow patterns of unmanned traffic management (UTM) airspace by analyzing simulated historical data. Mission patterns are characterized and identified by considering multiple UAV missions and scenarios with different priority levels to highlight UAVs' trajectories and deviations from the actual path due to these constraints. The pertinent data analysis supports risk analysis and improves trajectory planning in different airspace regions considering all dynamic parameters such as extreme weather, emergency services, and dynamic airspace structures. The data processing framework, which is density-based spatial clustering of applications with noise (DBSCAN), identified significant deviations in mission patterns with almost 82% confidence level. The UTM traffic flow characterization is conducted by three key characterization parameters mainly Distance from Centroid (DFC), Distance to Complete Mission (DTCM) and Time to Complete Mission (TTCM). This work also analyzed the airspace congestion using the Kernel density estimation (KDE). This analysis identified some regions of interference as potential congested areas representing safety concerns. The proposed framework is envisioned to assist UTM authority by characterizing air traffic behavior, managing its flow, improving airspace design, and providing the basis for developing predictive capabilities that support traffic flow management.

INDEX TERMS Machine learning, traffic flows patterns, trajectory data analytics, unmanned traffic management.

I. INTRODUCTION

Research techniques addressing the problem solutions in application domains involving multiple unmanned aerial vehicle (UAV) missions have significantly increased in recent decades. UAVs represent the future evolution of the aviation industry, and their usage is significantly increasing in many aspects of people's lives. In recent times, the civilian applications of UAVs have risen across diverse fields due to their versatile functionality, automation capabilities and low cost. The application areas of UAVs for both consumer and industry include business and marketing, surveying and monitoring, emergency services and healthcare, delivery services, gaming and sports telecasting, news reporting, the education sector, military, security, and many other fields [1], [2].

Although UAVs have many advantages, they face limitations if their routes are not managed and operated by a high-level automation system. In the absence of such a system, flight operations in airspace can imperil the security, safety, and privacy of the public. To carry out UAV missions and

The associate editor coordinating the review of this manuscript and approving it for publication was Amin Zehtabian.

other manned aircraft operations safely, a systematic integration of UAVs is required in the National Airspace System (NAS) before using them for civilian purposes [3].

The mid-air collision over Grand Canyon in 1956 is considered as the real cause for the development of the air traffic management (ATM) system that is used nowadays. The development of an ATM-like system is becoming necessary to ensure the safety of civilian UAV operations at lower altitudes [4]. The ATM is fragmented at the technological, operational and functional levels, and their integration is needed to increase safety, improve efficiency and reduce environmental impacts on the atmosphere [5]. The key parameters for the integration of UAVs with manned aircrafts in a shared airspace includes autonomous collision detection, sensing, awareness and avoidance [6], [7].

Factoring in the above concerns, unmanned traffic management (UTM) is designed to carry out the management of UAS operations economically, efficiently and safely, and it is considered a subset of air traffic management. It is also defined as a system of systems (SoS) developed using users' cooperation as well as their systems [8]. The ultimate objective of UTM is to carry out efficient and safe low-altitude aerial operations by providing different services. These UTM services include spacing and sequencing, dynamic geo-fencing, route planning and re-routing, dynamic configuration and airspace designing, contingency management, terrain avoidance, severe wind and weather avoidance, separation management, and contingency and congestion management [9]. Since a number of the above services rely on trajectory data, the field of trajectory data mining and data analytics is seeing a growing interest in the UTM context.

The aviation industry uses flight-tracking data heavily and conducts research using advanced data analytics tools and technologies with an aim to characterize the air traffic behavior for monitoring airspace, managing air traffic flow, carrying out performance assessment and improving airspace design [10]. Oliver et al [11] detected and identified particular events in a huge amount of historical aircraft-trajectory data, and it falls under the scope of information extraction and knowledge discovery. Olive and Basora [12] highlighted the usage of data mining in the ATM context by suggesting that it helps sort out the desired information from the huge amounts of data generated daily by various stakeholders of the ATM systems. This information sorted from the generated data is beneficial for different stakeholders for specific purposes: an air navigation service provider (ANSP) may enhance capacity indicators; commercial stakeholders like airports and airlines may improve short-term predictions and optimize their operations; academic stakeholders may design better safety models and make better risk estimations; and air traffic control (ATC) training centers may carry out more realistic simulations.

Although, the ATM domain is extensively studied, limited studies have been conducted in the UTM context. This is due to an excessive on the implementation and control approaches of UAVs [13]. Moreover, a considerable barrier to data analysis in UTM is the absence of a common and shared database containing real-time UAV flight-operation data. One possible development direction is to use simulation data [14].

Since UTM airspace constitutes less-densely populated small urban areas, there is a strong demand to study and characterize UTM traffic flow behavior that cover the whole routes. Further, there is a need to evaluate UTM airspace congestions to address the safety aspects that have not been analyzed yet. Moreover, the impact of dynamic factors like adverse weather conditions, emergency operations, the combination of static and dynamic obstacles to discover feasible rerouting options through air traffic flow patterns studies have not been studied previously.

Thus, the current study proposes an unsupervised machine learning–based clustering framework for the detection and characterization of UAVs' trajectories. We performed the airspace congestion analysis using a Gaussian kernel density estimator. The following are our contributions in this regard:

1) Realistic UTM multi-services mission scenarios are designed, incorporating the effects of weather conditions and static and dynamic obstacles along with random UAV trajectories of flying hobbyists (recreational users) trajectories.
2) A UTM flight-trajectory data analytic framework is developed for the identification of UAV trajectory patterns at the spatial and temporal scale that uses an unsupervised machine learning (DBSCAN) algorithm.
3) Key Characterization Parameters (KCP) for modeling UTM mission-data traffic flows are introduced. These metrics are evaluated for worst-case weather scenarios and dynamic airspace constraints, in order to present deviations in UAV missions.
4) A Gaussian kernel density estimator–based airspace congestion analysis is performed to identify hot zones and regions of interference.

The rest of the paper is organized as follows: Section II presents related work and some background on the techniques used in this study. Section III discusses the proposed methodology of this work. Section IV presents the simulation scenarios and result. Section V discusses the airspace traffic pattern and density. Lastly, Section VI provides a conclusion of this paper and some guidelines for future work.

II. LITERATURE REVIEW AND RELATED WORK

A. OVERVIEW OF TRAJECTORY DATA MINING TECHNIQUES

Data mining helps extract beneficial information from enormous datasets and is commonly known as knowledge discovery [15]. Likewise, the primary objective of trajectory data mining is to discover relevant knowledge from trajectory datasets on traffic abnormality, travel behavior and movement patterns. Furthermore, trajectory data mining has two main goals: description and prediction. Description focuses on finding human-interpretable structures while illustrating the data, whereas in prediction, some variables are used in the data to ascertain the future values, unknowns and other

required variables [16]. Trajectory data mining has been regarded as a vibrant research area across various domains. Zheng [17] used data mining techniques to classify trajectory data into four categories: mobility of natural phenomena, mobility of transportation vehicles, mobility of animals, and mobility of people.

Several other studies have been conducted in the recent past that are based on air traffic datasets extracting valuable behavioral information of moving objects like animals, vehicles, and people [18]. Recently, many airlines established different divisions for analyzing flight safety and related issues based on historical data analysis. Additionally, many airlines are exploring new methods based on data science for improving their airline safety by analyzing traffic events from historical data [19]. Due to the availability of huge amounts of trajectory data from gadgets and other applications that use GPS, a number of surveys related to trajectory data mining have been conducted [20]. Parent et al. [21] provides an analysis of mobility data management, listing by discussing the main techniques for mining, enriching, building and extracting knowledge from trajectory data. The survey by Kong et al. [22] presents trajectory applications and data from travel patterns, travel behavior, trajectory data service description in terms of transport management, and other aspects. On the other hand, the survey by Bian et al. [23] proposes a set of trajectory clustering techniques, classifying them into three categories: supervised, semi-supervised and unsupervised.

Clustering is an unsupervised learning process. It is considered a first-tier trajectory mining method to determine heterogeneity and homogeneity based on data properties, and thus similarities within a trajectory dataset are revealed by dividing the trajectories into various clusters [24]. In a nutshell, the features of trajectories' movement must be same within a cluster, whereas features vary between clusters. Generally, each trajectory is represented by a feature vector, and later on, the similarity between trajectories is measured by finding the distance between their feature vectors [17].

To design a trajectory-specific clustering model, many efforts incorporating the features of trajectories have been made, and most of them are probabilistic and statistical models. Smyth and Gaffney [25] proposed a clustering approach based on mixture models that combines trajectories that are produced by a common representative trajectory with the addition of Gaussian noise. Similarly, Alon et al. [26] used a Hidden Markov Model (HMM) to model clusters because it fits the trajectories best, and trajectories are designed as sequences of transitions between different points. Clustering algorithms based on the similarity functions determine similar direction, similar source, similar route, and similar start and destination. In this regard, Maimon and Rokach [27] offered a detailed discussion on how to apply similarity functions and distance that further help in determining cluster membership.

Two well-known algorithms have been mentioned in this work. The first one is OPTICS (ordering points to identify the clustering structure) [28], and the second is DBSCAN (density-based spatial clustering of applications with noise) [29]. T-OPTICS [30], an extension of OPTICS, was designed by describing a spatiotemporal distance for clustering and comparing trajectories. On the other hand, ST-DBSCAN [31] was developed as an extension of DBSCAN to improve the identification of noise and clustering using two additional parameters. Depending on the similarity function and the goal of analysis, trajectory clustering can be applied on sections of trajectories or on whole trajectories. The route of trajectories is not important, so they can be clustered if their similarity function is validated on the basis of their similar origin and similar destination [32], [33].

Classification is the second trajectory data mining method. As it is a partially supervised or supervised learning process, it is different from clustering [34]. The classes of classification must be predefined. Moreover, a training set of objects are required to be pre-labelled based on their class. Two steps are needed for a typical trajectory classification algorithm. In the first step, a set of distinctive features are extracted for training an already existing standard classification model such as decision trees, support vector machine, nearest neighbors and logistic regression. In addition, the properties of the trajectory that suit best to describe different classes of trajectories are determined. In the second step, a significant standard classification model is selected, which is then applied to the already extracted distinctive features.

Many comparative studies have been done on various standard classification models [35]. These classical algorithms are directly applied for trajectory classification in most cases. Bolbol et al. [36] used Support Vector Machine (SVM) for transportation mode classification. The authors used statistical methods and assessed the distinctive power of some features of common transportation means such as, train, bicycle, subway, walking, and private car. They also determined the acceleration and speed of these means of transportation. In most cases, some pre-processing such as clustering, segmentation and statistical analysis were carried out to classify trajectories that produce those features required for classification.

Zheng et al. [37] proposed a change point–based segmentation method to divide each trajectory into distinct segments of non-identical transportation modes. The work identified a set of features that are not affected by altering traffic conditions. Patel et al. [38] emphasized on improving prediction accuracy by adding time duration information that helped differentiate dynamic objects moving at different velocities. Lee et al. [39] extracted sub-trajectory and regional trajectory features using SVM-based classification algorithm.

There are also other works related to discovery of movement patterns hidden in the trajectories. Mazimpaka and Timpf [40] discovered the spatial and temporal aspects of these mobility patterns. Nasreen et al [41] also associated the nomenclature for these movement patterns that include periodic patterns, associations, sequential rules, subgraphs and frequent items. Wachowicz et al [42] classified the movement patterns into three different kinds: swarm, convoy

and flock. According to this work, a group of objects is referred to as a flock if they move together for at least t successive timestamps and their locations can be observed in a disk of radius. A flock and convoy are quite similar to each other, with a convoy being dissimilar only for the disk shape. As long as the positions of the moving objects are clustered, any disk shape can be formed by a convoy pattern on each time slice. These patterns are clustered usually by density-based clustering with minimum object number and maximum neighborhood distance [43]. The requirements for a convoy are further relaxed by a swarm, and in this case, no object positions are required to be clustered in each time slice [44].

In every case involving swarms, convoys and flocks [16], collective pattern mining is done by density-based clustering, which is considered the most common method. The next section discusses the literature survey conducted in the field of data analytics for air traffic flow identifications.

B. FLIGHT DATA ANALYSIS AND TRAFFIC PATTERN IDENTIFICATION

The availability of historical traffic data has led to attention from research community to identify the trajectories and properties of air traffic [45]. For getting insights about the behavior of dynamic targets like animals, people and vehicles, sensing technologies have already been used in the past [46]. The usage of flight-tracking data in the aviation industry for applying advanced analytics methods has been investigated in several studies. In [10], the air traffic flow was characterized for better traffic flow management. The same type of study is conducted in [47] and [48] for better airspace design, airspace monitoring and performance assessment.

In [49], potential events were detected and identified by assessing the deviations in recorded trajectories' data. This study determined the efficiency of aircraft operations in a complex systemized terminal maneuvering region. The performance of aircraft operations is assessed in the area of London's multi-airports due to actual air traffic flow and standard route structures. Basically, this work falls under the domain of traffic pattern recognition and flight data analysis, particularly in the terminal maneuvering areas (TMA). The methodology followed in this work is comprised of two modules. The first module is termed as data-driven 4D (x, y, z, t) adherence calculation process. The ultimate objective of this process is to assess trajectory deviation, identify recurrent patterns and thus assess the 2D interdependencies of the standard routes and finally determine the high-demand routes. In the second module, concurrence events that may result in conflicts and can cause a lack of adherence are determined. Nonetheless, the above study has been able to give some insights about air-traffic flows by identifying their patterns, but more emphasis is on TMAs such as airports. Furthermore, it does not cover any UAV traffic flow within a densely populated low-dynamic airspace.

Murca et al. [50] applied various clustering methods to learn traffic flow patterns in both spatial and temporal dimensions. The authors analyzed these patterns for complex and super-dense metroplex airspace and estimated the predictability, capacity and efficiency of the metroplex. They also characterized the dynamics of air-traffic operations. Bombelli et al. [51] used clustering to identify general routing structures in US airspace enroute trajectories. Amerson et al. [52] applied trajectory clustering methods to estimate the effects of convective weather on flow rates and dominant routes between New York and Fort Worth centers. The ultimate goal of the above studies was to develop high-fidelity models and learn the actual traffic route network for better traffic flow management.

Ren and Li [53] compared flight trajectory data for China and US to learn the air traffic routes, and discovering airspace utilization patterns and some significant network structures. The horizontal efficiency of enroute flows was evaluated by Liu et al. [54], accomplished with the help of trajectory clustering for US airspace.

The authors estimated the horizontal efficiency by measuring the ratio between the length of the shortest routes and the real trajectory lengths. They also developed a statistical model to assess the impact of various parameters on trajectory inefficiency. It was observed in this study that the most significant causal factor for enroute inefficiencies is convective weather.

A number of clustering algorithms have been used in determining the spatial and temporal traffic patterns using flight data. The significant clustering methods that are widely used include OPTICS [28], Hierarchical Density-Based Spatial Clustering of Applications with Noise (HDBSCAN) [55], k-means [56], and DBSCAN [29].

Similarly, Samantha et. al. [57] also contributed to making modern aviation systems safer by means of high-precision trajectory prediction and robust anomaly detection methods. This work also focused on the terminal airspace trajectory prediction and anomaly detection methods by the identification of air traffic flows. Since the air traffic flow patterns are identified using clustering algorithms whose performance depends on the characterization of an appropriate distance function, the selection of this distance function like Euclidean distance becomes a challenge due to the divergent and convergent nature of traffic airflows within the terminal airspace. The novelty of this work is the adoption of a weighted Euclidean distance function to improve trajectory clustering within the terminal airspace. In this work, numerous weighting schemes were evaluated by applying the HDBSCAN algorithm to cluster the trajectories. The key finding in this work was that if the trajectory points closer to the border of the terminal airspace, but not necessarily at the border, are weighted highest, then a more accurate clustering is computed.

The above study determined air-traffic flows by identifying patterns in terminal maneuvering areas, and more emphasis was placed on optimizing a weighted distance function so that the best possible clustering is achieved. This study doesn't address any UAV traffic flows in the terminal maneuvering

areas within a densely populated low-altitude highly dynamic airspace.

In a PhD study [58], a flight trajectory data analytics framework was developed to provide a high-fidelity characterization of air traffic flows from large-scale aircraft-tracking data. This work applied machine learning methods to discover spatial and temporal trends in aircraft movement. The proposed framework allowed to automatically learn the airspace structure, assess the use of the airspace and identify patterns of airspace usage. For this, it included three modules: (1) clustering flight trajectories at the spatial scale to identify trajectory patterns, (2) trajectory classification by using Random Forests algorithm to assess flight trajectory conformance against the learned airspace structure and identify air traffic flows, (3) clustering air traffic flows at the temporal scale to identify traffic flow patterns. This framework was used to obtain a detailed characterization of air traffic flows in the terminal areas of multi-airport systems including New York, Hong Kong and Sao Paulo.

This work also highlighted the influence of weather conditions on airspace use and traffic performance and recommended the integration of weather forecasting in decision-making. It utilized the above data analytics conclusions to develop a data-driven approach for airport capacity planning towards an improved decision support system. This decision support system used predictive modelling for capacity estimation and prescriptive modelling for capacity allocations. The authors used a random forest–based supervised learning method to predict traffic flow patterns.

Although the above PhD thesis covered a lot of facets in air traffic flow prediction, it did not evaluate the enroute traffic behaviors and thus did not visualize the routing patterns between origin and destinations. Moreover, the impact of adverse weather conditions to discover feasible rerouting options were not addressed. Furthermore, the work did not cover the domain of TMA or enroute traffic patterns in the UTM context.

A novel framework for analyzing air traffic flow was proposed in [59]. This framework is based on hierarchical density-based spatial clustering of applications with noise (HDBSCAN), an improved version of the clustering algorithm DBSCAN. A single input parameter is used to manage clusters of distinctive densities in this improved version. In this study, two methods – symmetrized segment-path distance (SSPD) and Euclidean distance (ED) – that are based on two different distance functions were evaluated. Traffic patterns in both terminal and enroute areas are widely analyzed using this framework; thus, it is a quite useful framework.

Although this work employed a new dynamic clustering algorithm for predicting air traffic flows, the focus is on the distance function selection for better optimization results. HDBSCAN may be utilized for clustering UTM data traffic flow to consider the effects of noise.

Air traffic trajectories can be separated by an approach used in [60], carried out in a constrained area through operational procedures. In the Toulouse terminal maneuvering area, the clustering algorithm is applied on a set of real trajectories. It is observed that a better understanding of traffic structure can be achieved by a DBSCAN-based clustering method, and schedule landings of aircrafts can be controlled at Toulouse–Blagnac Airport. A cluster of significant trajectories with useful information has also been identified through this study. Moreover, these trajectories are paving the way for a probabilistic approach to carry out risk assessment in air traffic. Although this work validated the use of DBSCAN-based data analytics methodology for air traffic flow separations, it did not disclose any specific patterns' classification and the scope of terminal maneuvering areas in ATM space.

The scope of analysis in all previously mentioned studies is constrained to air traffic management and does not take into account the challenges in the UTM context. Furthermore, in operational performance analysis, the influence of airspace structure is generally disregarded in older works. Moreover, the effect of weather conditions in defining air traffic flows has been examined in few studies. To compare and characterize the air traffic performance at various scales, the entire flight trajectory has been considered in our work, in contrast with previous works, and includes terminal maneuvering areas and enroute trajectories for UTM airspace.

III. METHODOLOGY

A. SIMULATION SETUP

The suggested methodology is evaluated and verified by running simulations for the airspace of Bedfordshire, UK. TABLE 1 depicts places that may be restricted for flights, such as airfields, recreational areas and prison. They include four airfields: Luton, Cranfield, Halton and Old Warren (Orange), four recreational areas: Dunstable, Sandy, Cardington and Graveley (Yellow), and Milton Keynes Prison (Blue). The blue color trajectory corresponds to Covid-19 sample missions by UAVs (1,2,3), the magenta color trajectory shapes represent the package delivery service by UAV-4. The cyan color trajectory represents the package delivery service by UAV-5. The red color trajectory presents the fire surveillance missions, and the black lines belong to recreational users. To make the simulation more realistic, the following simulation parameters are taken into consideration:

1) Structure of airspace: Our simulation framework does not allow us to simulate ascending and descending maneuver; thus, the cruise phase of UAVs has been displayed exclusively in 2D (x, y).
2) Fixed start and end position: As part of the simulation, the UAV-mission start and end positions have been set to mimic typical everyday operations and emergency services.
3) Priority levels: Due to the urgency of some flights, it is necessary to prioritize these over less pressing services. For instance, this is relevant for emergency service flights, including air ambulances or search and rescue services, which require the ability to move freely

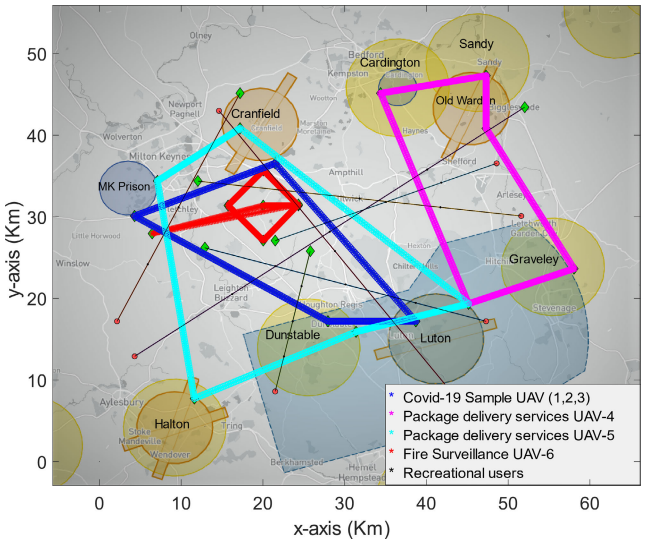

FIGURE 1. Simulation environment created by air map.

in the airspace and have fast, effective responses when involved in conflicts. In light of this, NASA UTM proposed, in its ''prioritization'' recommendation, that each aircraft service receives a varied priority level [61]. Specifically, the U-space recommendation wished to introduce eight priority levels, numbered between one and eight, where eight is the lowest priority [62]. In this study, each flight has been assigned a service priority level, ranging from level 1 (highest priority) to level 4 (lowest priority). The following is a description of each level of priority:

1. Fire surveillance services using loiters' trajectory patterns.
2. COVID-19 sample test delivery service to multiple clinics.
3. Package delivery service from multiple post offices.
4. Recreational UAV user (hobbyist flyers).

4) Dynamic no fly zones (NFZs): In some hours, airfields and recreation areas considered for simulation are dynamic in nature. This dynamism is random, making some areas available and others unavailable during the whole hour.
5) Random departure time: To make the system more realistic, the exact time at which each hobbyist's UAV departs is set randomly between 1 and 10 minutes in a 1-hour simulation scenario period.
6) Weather ambiguity: We have considered different weather conditions classified as adverse and severe.

During flight planning and implementation, as well as post-flight actions, a UTM infrastructure is able to deliver specific services to operators. Such services include flight planning, electronic identification, approving flights, managing airspace capacity, geofencing, UAV tracking, airspace dynamic information, meteorological information, providing support in conflict detection, manned air traffic management interfaces [63]. The UTM infrastructure ultimately requires the use of drones to be able to effectively exchange information continuously with these services, and this requires strong, consistent, and low-latency Drone-to-Infrastructure (D2I) communication data links. A comprehensive evaluation and performance study is presented in [64], considering particular communication challenges like channel modelling, physical layer techniques, and security, etc. However, the applied communication channel aspects that may be hindered during highly dense UTM operations are not considered in this work. In this study, we assumed that the bandwidth is sufficient to meet the UAVs' rate requirements and interference is trivial as different users and UAVs use different frequencies. We have assumed throughout this work that there are no communication blackouts and there is a uniform communication performance across all areas. This underpins the focus of our work, where this paper proposes a data analytics framework to characterize traffic flow patterns of unmanned traffic management (UTM) airspace by analyzing simulated historical data.

B. PATH PLANNIG OPTIMSATION

Path planning is the most critical research area focusing on determining an optimal path between UAVs' source and destination. UAVs may come across several obstacles during their operations in a dynamic environment, the path should be determined in such a way that there should be no collisions between the UAV and its surrounding obstacle [65]. The major challenges for an optimal path planning of UAVs are listed in [66]. Several research approaches have been proposed in recent years that describe path planning of UAVs and address different issues. Researchers focus on different path planning issues of UAVs in context to the complexity and shape of UAVs. The authors of [67], for example, assessed coverage approaches and found that they are categorized according to a classical taxonomy, including precise cellular decomposition, no decomposition, and estimated cellular decomposition. Various shapes of the area of interest, for instance, rectangular, concave, and convex polygons, are also considered here. Through the years, computer vision technology has progressed to the point that it facilitates UAV localization as well as obstacle detection and avoidance. Al-Kaff et al. [68] presented a broad review of computer vision algorithms and their applications for the autonomous navigation of UAVs. A comprehensive analysis on the execution of computer vision technologies for control, tracking, navigation, and obstacle avoidance of UAVs was given by Lidia et al [69]. Artificial Intelligence (AI) is being put into operation in UAVs navigation systems in conjunction with computer vision technology to allow them to develop humanoid awareness. The nonlinear trajectory is addressed by a novel Deep Reinforcement Learning approach to manage numerous UAVs with the overall goal to track multiple first responders (FRs) throughout challenging 3D environments, including those with a range of obstacles and occlusions, as proposed in [70].

The non-availability of historic UTM traffic data prompts the generation of data for the analysis of UAV traffic flow patterns using a simulation framework. In this work, particle swarm optimization (PSO) is utilized to provide optimal paths from a UAV service start point to the delivery point. PSO is a stochastic optimization method that was developed by J. Kennedy and R. Eberhart in 1995. It is a swarm intelligence–based metaheuristic algorithm capable of tackling complicated mathematical problems in engineering [71]. The main advantages of PSO are that it is simple to understand, easy to implement, and converges rapidly compare with other traditional global optimisation methods such as genetic algorithms and simulated annealing [72]. PSO is useful for estimating and optimizing trajectories from point A to point B. As a result, PSO can track an optimal trajectory while using the least resources possible and avoiding every obstacle and NFZ.

C. WEATHER EFFECTS' IMPLEMENTATION

For a UAV's operation, weather hazards are classified into moderate, adverse and severe [73]. Moderate hazards are those that result from phenomena that reduce visibility but do not harm the aircraft. Severe weather hazards are those that might cause significant damage to an aircraft or result in its loss of control. Adverse hazards weather conditions that have potential to cause loss of control, loss of communication and diminished aerodynamic performance and may negatively affect the operator. Thus, it is well accepted that flying in severe weather should be avoided. The weather has a massive impact on UAVs' operation. Different types of inclement weather can have a significant impact on a UAV, which are mentioned below.

1) PRECIPITATION

Precipitation can negatively affect the operation of a UAV by water getting inside and ruining electrical components [73]. This will make a UAV completely inoperable and cause it to crash. To deal with the adverse precipitation, UAVs should have proper insulation. The weight of water on the UAV's wings due to rain can be used to evaluate the deviations in UAV waypoints from the planned trajectory caused by rainfall. The value of precipitation at each cm^2 area is low when the UAV flies in moderate rain. The small amount of water falling from a UAV's wing will add a less amount of water weight to the total weight of the UAV and rainwater. If the precipitation is heavy, the amount of rain falling on the UAV's wings per cm^2 area causes an imbalance in the weights of left and right wings. Equation (1) gives the imbalance of weight expressed as:

$$\omega_w = \omega_s + \omega_r \tag{1}$$

where ω_w represents the UAV's wings' accumulative weight, ω_s is the structured weight, and ω_r is the water weight on the UAV's wings' due to rain. ω_r is further classified into the total water weight on each wing ω_p and the weight of water falling from the UAV's wings' ω_f. The mathematical representation of ω_r yields:

$$\omega_r = \omega_p - \omega_f \tag{2}$$

The precipitation-caused deviation of way points from the planned trajectory is directly proportional to the UAV's wing areas. When subjected to precipitation, the rotary wing of the UAV shows more resistance as compared with the fixed wing to the deviation.

TABLE 1. Scale of weather classifications used in this study.

Weather types	Adverse	Severe
Wind (m/s)	13–23	> 33
Rainfall (mm)	3.0–7.0	Above 7.45

2) WIND

Drones can be blown off course by strong winds, making them impossible to control during takeoff, in-flight, or landing, thus resulting in a crash. When the wind direction is normal to the direction of the UAV, the wind forces the UAV to change its trajectory [74]. Strong winds have the potential to affect an unmanned aircraft's ground speed and flight path. Wind speeds can easily exceed the maximum speeds of UAVs, unlike manned aircrafts. Fixed-wing UAVs have an aerodynamic structure that helps them maneuver through air streamlines, whereas even at lower wind speeds, rotary-wing UAVs are more likely to struggle. That is why fixed-wing UAVs have a higher maximum speed than rotary-wing UAVs [73]. The mathematical representation of high-speed winds' impact on the operation of UAV is presented as follows:

Suppose the direction of wind is denoted by β_1, and the deviation in a UAV's trajectory caused by the wind is denoted by β_2. m_1 and m_2 are vertical line equations slope. The relationship between the slopes and directions of wind and the deviation of the UAV is as follows:

$$m_1 = tan\beta_1 \tag{3}$$

And

$$m_2 = \frac{y(z+1) - y(z)}{x(z+1) - x(z)} \tag{4}$$

where z is the simulation discretized steps. A vertical line is formed at the instant the UAV interacts with the wind at every step. The change in direction along x-axis and y-axis is defined by:

$$x = \cos\beta_2, \quad y = \sin\beta_2 \tag{5}$$

$$Tan\beta_2 = \frac{(m_2 - m_1)}{(1 + (m_2)\,(m_1))} \tag{6}$$

Table 1 shows two different weather classifications based on the Beaufort wind scale and rainfall precipitation.

D. DECONFLICTION STRATEGY

As the number of UAV operations increase, it is vital to implement effective measures for managing airspace conflicts by preventing two or more UAVs from operating in the same place simultaneously. These conflicts are high-risk scenarios that may result in damage to assets or human fatalities.

The NASA UTM recommendation aims to allow UAV operators to prevent these airspace conflicts by accurately exchanging information through supporting services. This concept, known as strategic deconfliction, is the first of three layers that form the conflict management model laid out in the recommendation, with the other two layers being separate provision and collision avoidance. The key notion surrounding this first layer is prioritization, which involves designating priorities using the UTM system and handling UAV operations in such a way as to improve situational awareness and encourage more communication between airspace users. To resolve potential UAV conflicts, our recent work [75] outlined some possible deconfliction strategies, which consider the UAV priority mechanism we previously mentioned.

E. FRAMEWORK FOR CHARACTERIZATION OF AIR TRAFFIC PATTERN

For the identification and characterization of UAV traffic flow patterns, a flight trajectory–based framework that uses the DBSCAN algorithm, and the Gaussian kernel density estimator has been described here. Since the UTM traffic flows are related to UAV missions following the same trajectory paths on different time schedules, deviations in the planned paths are expected due to the presence of dynamic airspace architectures, weather uncertainties and random hobbyist flights. The characterization of traffic flows thus needs the detection of trajectory patterns for each mission separately for characterization. In the past, a number of researchers have conducted ATM traffic-flow pattern identifications, using DBSCAN for terminal-maneuvering areas around airports [49], [50], [58], [59], [60] as already discussed in section II-B. Our proposed framework comprises the following functions:

1) DBSCAN–based clustering of UAV trajectories in the spatial domain.
2) Identification of UAV mission-based clustered groups.
3) Statistical analysis of noisy cluster groups and valid mission trajectories.
    1. Valid clusters are clusters that belong to the class of one of the three planned missions.
    2. Noisy clusters are clusters that pertain to random flying of UAVs by hobbyists.
4) Characterization of UTM traffic flows using detected mission clusters.
5) Congestion analysis of UTM airspace Using a Gaussian kernel density estimator for UAV trajectories.

This framework uses the above functions to automatically learn and identify the airspace structure. The main purpose

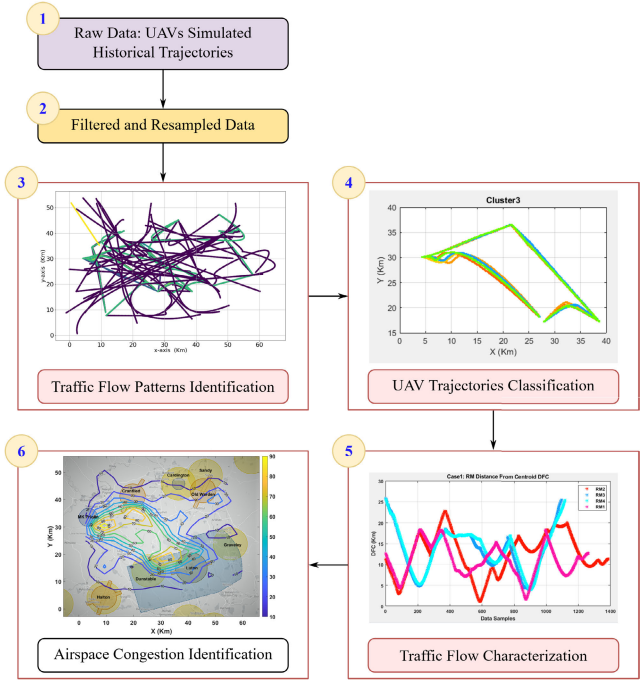

FIGURE 2. Overview of the UTM airspace characterization approach.

of trajectory clustering is to find groups of trajectories in the spatial dimension that belong to valid missions in the presence of random and dynamic factors. The framework also helps to find congestion patterns in the UTM airspace through calculations of air traffic density. The methodology of the above-stated flight trajectory framework for the characterization of air traffic flow for UTM is shown in TABLE 2.

Clustering tasks can be performed using a variety of approaches and algorithms, which can be classified into three sub-categories: partition-based (k-means), hierarchical (divisive, agglomerative) and density-based (DBSCAN). With normal-shaped clusters, hierarchical- and partition-based clustering techniques are extremely helpful. DBSCAN, on the other hand, is more efficient in detecting outliers or arbitrarily shaped clusters. In the presence of abnormal trajectory profiles, DBSCAN identifies the core trajectory patterns. It has ability to identify non-convex clusters and eliminate the need to predetermine the number of clusters.

In this study, DBSCAN is chosen because of two reasons: (a) the algorithm can decide the number of clusters automatically, and (b) outliers can be identified. These characteristics meet the requirement of trajectory clustering because (1) the number of typical UAV air traffic flow patterns is unknown with random factors such as dynamic objects, wind and random flights of UAV hobbyists, (2) UAV flights undergoing abnormal deviation can also be extracted from clusters as outliers. Successful applications of DBSCAN in air transport research can be found in the literature [76], [53].

DBSCAN clustering depends on the input parameters epsilon and minPts [58] as follows:

1) Epsilon: Distance threshold. It specifies neighbor distance. If the distance between two points is less than or equal to epsilon, then it is considered neighbor.
2) Minimum points (minPts): For defining cluster, minimum number of data points.

Core points, border points and outliers are defined based on the above parameters:

1) Core point: A point is considered core point if it is surrounded by at least minPts points (including the point itself) within the epsilon radius.
2) Border point: It is part of a cluster because it is within the epsilon of the core points, but it doesn't meet the criterion of minPts.
3) Outlier: When the point is not a core point and is also unreachable from any core point, then it is called an outlier.

The clustering process works on three main concepts, namely epsilon neighborhood, density reachability, and density connectivity, given below:

The D_i observation epsilon neighborhood contains all observations that are within the epsilon distance:

$$N_\varepsilon(D_i) = \{D_J \in Z / d(D_i, D_j) \leq \varepsilon$$
$$E_d(D_i, D_j) = \|D_i - D_j\|_2 \quad (7)$$

where D_i and D_j are two different trajectories taken from (7), and ε represents epsilon. The observation trajectory D_J is the density reachable from D_i if

$$D_J \in N_\varepsilon(D_i)$$
$$|N_\varepsilon(D_i)| \geq minPts \quad (8)$$

If there is chain of $D_i, \ldots, D_J$ such that each subsequent observation is directly density-reachable from the preceding one, then D_J is density-reachable from D_i.

D_J is the density connected to observation D_i if both observations are density-reachable from another observation D_k.

The algorithm begins with an arbitrary database instance and determines its epsilon neighborhood. Observation and neighborhood start clustering if it contains at least minPts, which is the core-point condition. The same procedure is applied for the neighbor's ε–neighborhood iteratively retrieved until the border points are achieved, or else the observation is classified as noise, and the algorithm moves on to the next database instance. If there are newly discovered core points, then this observation instantly labelled as noise can become part of the cluster, and the points are defined as density-connected points. TABLE 3 illustrates the DBSCAN concept.

The following methodology is adopted in this regard:

1) Pre-processing data by resampling the data for better resolution.
2) Tuning the DBSCAN parameters heuristically for extracting valid mission trajectories as one cluster or class.
3) Labelling different cluster groups pertaining to one mission.

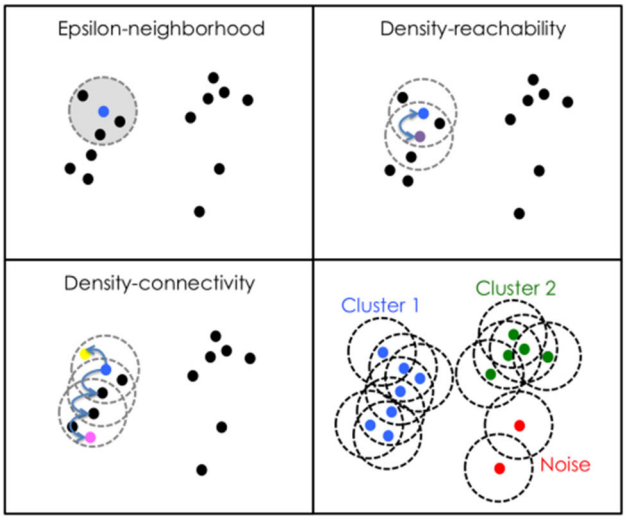

FIGURE 3. DBSCAN clustering [58].

4) Visualizing the group of mission clusters as aggregate or combined plots for identifying different deviation patterns for each mission.
5) Reporting the statistics of trajectory points per cluster.
6) Calculating the percentages of valid and noisy clusters.

Since the data is generated using the PSO simulation framework, no data filtering is required; however, for the sake of better resolution, the trajectory data for 100 UAVs with 100 interpolated sample points is up-sampled to about more than 20000 sample points for smooth DBSCAN clustering. The DBSCAN algorithm is applied for the clustering and classification of the above mixed-mission data for three scenarios; further details are provided in the following section. Google Colab–based Python environment is used to run the DBSCAN clustering algorithm. The parameters epsilon (ε) and minimum points (**minPts**) are tuned for each dataset accordingly, in order to acquire better results. In this manner, different mission-trajectory patterns are identified in this unsupervised learning mechanism.

Additionally, the hobbyists' single-leg trajectories were identified as outliers in this work. The clustering for these scenarios is tuned and achieved with different epsilon (ε) and minimum points (minPts) using the heuristic method are presented in Table 2.

Once the clustering is done using the DBSCAN algorithm, a detailed cluster analysis is conducted using the trajectory matrix and labelled clusters to visualize different mission trajectory patterns and their shapes. Furthermore, aggregate or combined cluster patterns for different missions are plotted and analyzed. The analysis is also supported with the help of the percentage of valid and noisy clusters found using DBSCAN. The tally of different trajectory patterns of various missions is also obtained. We further evaluated the percentages of various valid mission trajectories detected per cluster in this analysis using pie charts.

TABLE 2. DBSCAN cluster's parameters for simulation scenarios.

Scenario	DBSCAN Parameters		Total Clusters	Valid Mission Clusters	Noisy Clusters
	eps	minPts			
0	0.6	3	11	9	2
1	0.6	3	9	7	2
2	0.6	3	7	5	2
3	0.4	3	12	7	5

IV. SIMULATION SCENARIO AND RESULTS

A significant amount of research has been conducted on the use of UAVs in emergencies, for e.g., where they are used to transport much-needed medical supplies, food and water to a flooded area [77]. This indicates that academics are becoming more interested in UAV-assisted disaster management [78]. There is special need to develop scenario-driven planning approaches that aim to optimize plans for UAVs and enable the selection of who to serve, which routes to take and how much to deliver [79]. Due to limited resources and other restrictions, planning a relief operation is difficult, particularly for last mile delivery activities (from distribution centers to beneficiaries) [80]. A requirement for ''empirically grounded analytical modelling papers'' in the domain of research on disaster relief operations have been distinguished in [81].

To present our problem, we considered diverse situations that includes COVID-19 sample delivery to multiple-clinics. We also consider the Royal mail delivery along with square loitering-based fire surveillance missions. Furthermore, we considered the situations where flying hobbyists are flying their UAVs within the same time frames.

It is assumed that the Luton–Bedfordshire National Health Service (NHS) hospital is currently housing a fleet of three UAVs (UAV1, UAV2, and UAV3) for COVID-19 sample test delivery missions to multiple clinics in a defined distribution network. The UAVs' shuttle service will occur each hour. The delivery of mail packages is from Luton central delivery office to the multiple-post office. This mission fleet consists of two UAVs (UAV4, UAV5); one UAV will be allocated for the areas of Graveley, Old Warren, Sandy and Cardington, the second UAV will cover the remaining areas (Cranfield, Halton, Dunstable, and Milton Keynes Prison. The purpose of the central mail office to use two UAVs for delivering packages to multiple post offices is to reduce delivery time and gain customer satisfaction.

The firefighting-based rescue operations rely heavily on the surveillance operation using cameras. The initial videos and pictures taken by the payload cameras would help define the course of action in fire-fighting operations. Currently, only one square loiters operation is considered in our scenario. We are considering a UAV-6 available at Milton Keynes Prison Fire Station as a base station for these missions.

We are also considering where hobbyists are flying their UAVs along with the above-planned missions in this scenario. We assume these flying trajectories with one leg and random start and finish locations. The plan and schedule for each mission are presented in Table 3 below.

TABLE 3. The description and schedule for uavs missions.

Mission	Mission 1 COVID delivery sample test	Mission 2 Royal Mail packages delivery	Mission 3 Fire Fighting (Surveillance)	Mission 4 UAV flying by hobbyists
Trajectories number	36	30	6	28
Priority	2	3	1	4

TABLE 4. Technical parameters of UAVs.

Parameters of UAVs	Value	Unit
UAV type	Rotary-wing	--
Payload capacity	25	kg
Flight time	30	minutes
Cruise Speed	90	km/h
Wind resistance	10	m/s

We also assume that the UAVs are available at zero time and flying at constant speeds of 90 km/hr. It is further supposed that the times of delivery depend on the sequence of customers to be served along flight routes. Breakdown and maintenance times and costs are not considered. Each UAV follows a particular route, starting and ending at the same depot; the mission of a UAV is completed when it completely follows the assigned route and reaches back to the depot safely. To simulate more complex dynamic airspace, we considered 100 UAV trajectories, out of which 73 belong to special UAV missions and 27 for the random flights by hobbyists. Technical parameters of the UAVs are presented in Table 4.

We have simulated a multi-mission scenario between 9:00 am to 12:00 pm for the Bedfordshire area where four missions were taking place. Three different sub-scenarios were created based on these hours as follows:

A. SCENARIO 1–NFZs WITH NO WEATHER CONSTARINT AND DYNAMIC OBASTACLES

This simulation runs between 9:00 am and 10:00 am in the environment illustrated in FIGURE 4. In this simulated scenario, all nine NFZs are static with no dynamic obstacles and no weather constraints. As a result, no UAV could fly over four airfields, four recreational areas and one prison. However, any missions related delivery can be accomplished for these regions if applicable. The recreational users however are prohibited to fly over these NFZs.

B. SCENARIO 2–STATIC AIRFIELD AND DYNAMIC RECREATIONAL AREA WITH EXTREME WEATHER CONDITIONS

The second simulation scenario runs between 10:00 am and 11:00 am. The difference with the first scenario is that any

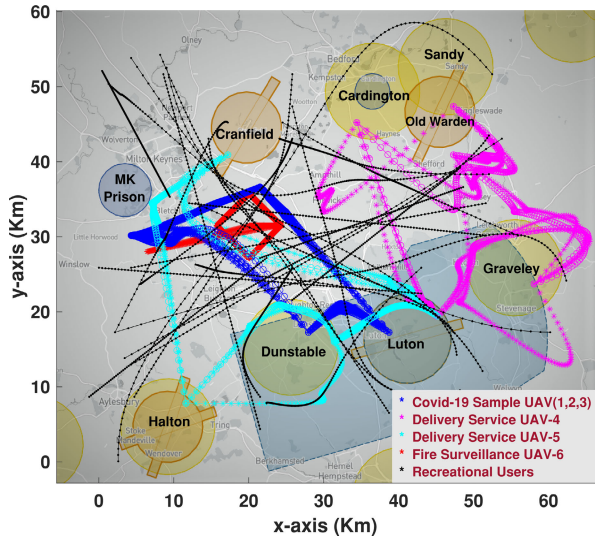

FIGURE 4. Simulation scenario 9:00 am to 10:00 am.

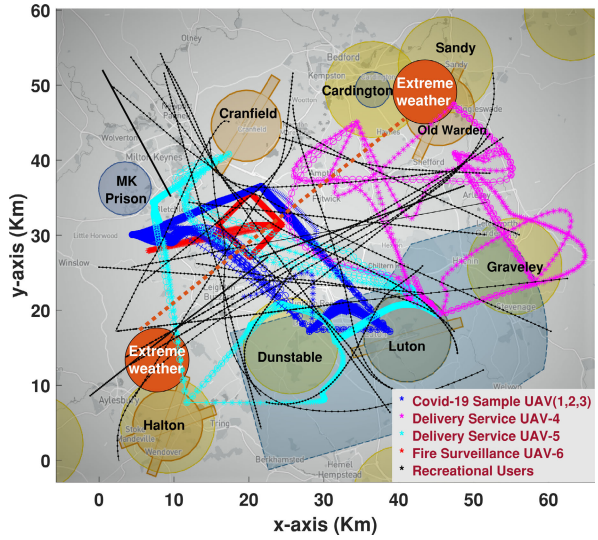

FIGURE 5. Simulation scenario 10:00 am to 11:00 am.

NFZ corresponding with recreational areas are dynamic, making some areas available and others unavailable in this hour. FIGURE 5 shows Dunstable, Sandy, Cardington and Graveley opened their airspace. Therefore, some UAVs could fly over dynamic NFZs during the simulation time. This scenario also incorporated the effects of extreme weather, dynamic in spatio-temporal axes, which would result in severe damage or loss of control of an UAV. Changes in extreme weather condition make it practically impossible to finish the flight of UAVs and have a significant impact on the success of planned missions of surveillance and COVID-19 sample distribution. Thus, UAVs avoid flying in extreme weather.

C. SCENARIO 3—DYNAMIC AIRFIELD AND STATIC RECREATIONAL AREA WITH DIFFERENT WEATHER CONDITION (RAIN AND WIND)

In this simulated scenario, airfields are dynamic, while all four recreational areas and the prison is kept static. Among

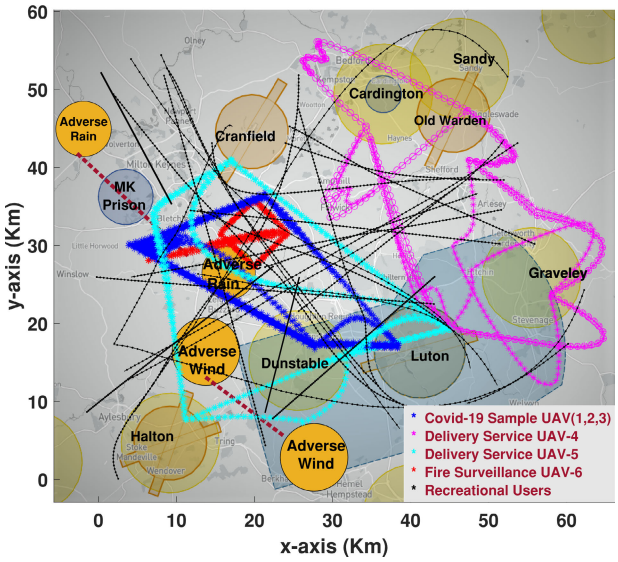

FIGURE 6. Simulation scenario from 11:00 am to 12:00 pm.

the four airfields, Luton and Cranfield airfields are available, as shown, and therefore UAVs of flying hobbyists can fly over Luton and Cranfield areas at some points. This scenario takes place between 11:00 am and 12:00 pm. Effects of adverse rain and wind have been considered, as shown in FIGURE 6.

V. AIRSPACE TRAFFIC FLOW PATTERNS, CHARACTERIZATION AND DENSITY DISCUSSION

A. IDENTIFICATION OF UTM AIR TRAFFIC PATTERNS USING DBSCAN

This section defines the results of identifying different trajectory patterns in the planned UAV missions explained in section IV above. The mission legs and their trajectories are shown in FIGURE 4, FIGURE 5 and FIGURE 6 under three different scenarios. These three scenarios perturb the ideal mission plans with the introduction of various dynamic random factors such as recreational areas, airfields and different uncertain weather conditions that cause trajectory deviations and result in different mission trajectory patterns that can't be identified visually.

An ideal case scenario was also simulated to create a reference UAV mission trajectory pattern that considers the whole airspace open without any static or dynamic obstacles and weather constraints. The results and analysis for the ideal case scenario and three main scenarios is narrated below:

1) SCENARIO 0—IDEAL CASE WITHOUT NFZ, WEATHER CONSTRAINTS AND DYNAMIC OBSTACLES

The intent of the DBSCAN clustering in our work is to assign trajectories to clusters in an unsupervised way similar to [50] and [82], thus identifying and separating the regular mission trajectories within the noise of recreational hobbyist missions. The input features used in DBSCAN-based trajectories clustering are 2D horizontal position vectors (X, Y) of all UAVs. These feature data are resampled to increase

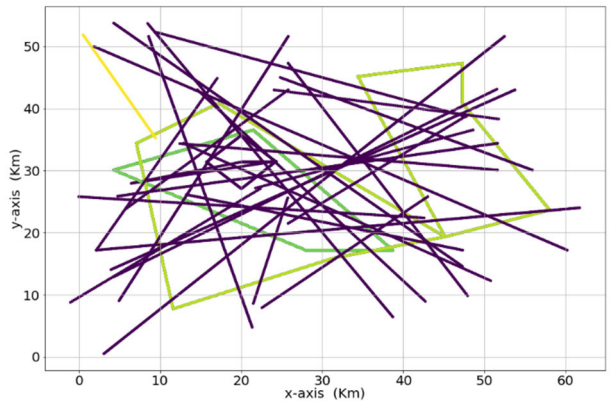

FIGURE 7. Scenario-0 DBSCAN results.

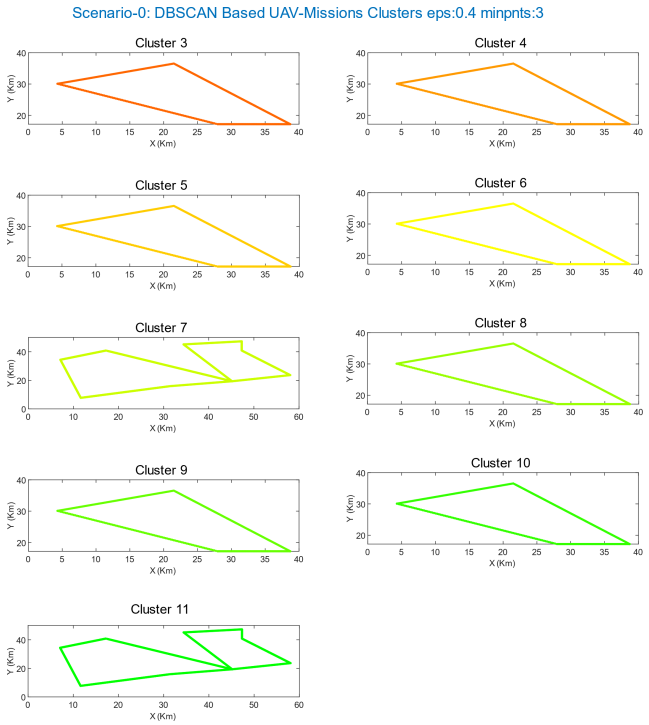

FIGURE 8. Scenario-0 DBSCAN detected mission cluster plots.

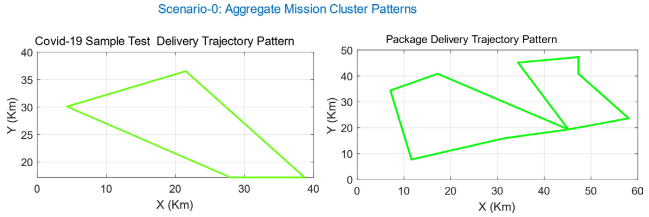

FIGURE 9. Scenario-0 detected combined mission patterns.

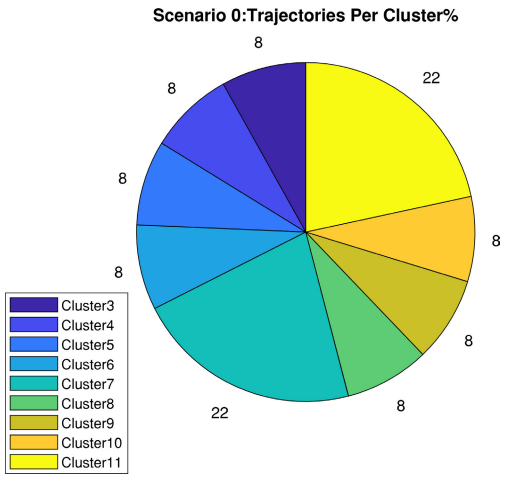

FIGURE 10. Scenario-0 trajectory count per cluster (%).

the resolution and provide equal spacing between consecutive trajectory points of each UAV. The regular mission trajectories (Covid-19 sample delivery and package delivery services) form regular shapes such as rectangles and trapezia through interconnected straight-line segments, while the recreational flyer's missions are shown as straight-line segments. The DBSCAN has successfully detected regular missions from the provided trajectory data set of the whole airspace without prior knowledge of any mission. The DBSCAN clustering results explicitly show the separate detection of UAV missions as line segments in different colors, such as dark green, light green, and yellow, while the recreational UAV users (hobbyist flyers) are detected and shown as line segments marked as noise (outliers) cluster group in violet color.

The clustering for this scenario is tuned and achieved with epsilon ($\varepsilon = 0.6$) and minimum points (minPts $= 3$). The detailed low-level clustered trajectory patterns detected with the above classifiers are depicted in FIGURE 7. It can be observed from the separated cluster graphs in FIGURE 8 that COVID-19 shuttle service trajectory patterns (UAV1, UAV2, UAV3) are detected with much higher numbers in clusters 3, 4, 5, 6, 8, 9, and 10. Also, the UAV4 and UAV5 package delivery service trajectory patterns are well detected and separated (clusters 7,11) from the denser areas where the outliers (such as random UAVs flying) have covered the airspace more comprehensively. Two types of trapezoidal trajectory patterns were detected, as shown in FIGURE 9.

We also evaluated the percentages of trajectory points per cluster for Scenario-0 as shown in FIGURE 10 below. It is evident that most of the trajectories detected are of the COVID-19 sample delivery missions as shuttle service with 56% weightage compared with delivery package services that constitute 44% of the trajectories of missions.

2) SCENARIO 1—NFZ WITH NO WEATHER CONSTRAINTS AND NO DYNAMIC OBSTACLES

The detailed low-level clustered trajectory patterns detected with the above classifiers are shown in FIGURE 11. It can be observed from the separated cluster graphs (FIGURE 12) that UAV1, UAV2, and UAV3 COVID-19 shuttle service trajectory patterns are detected with a much higher confidence level in clusters 3, 4, 5, 6 and 9. UAV4 and UAV5 package delivery service trajectory patterns are detected in clusters 7 and 8.

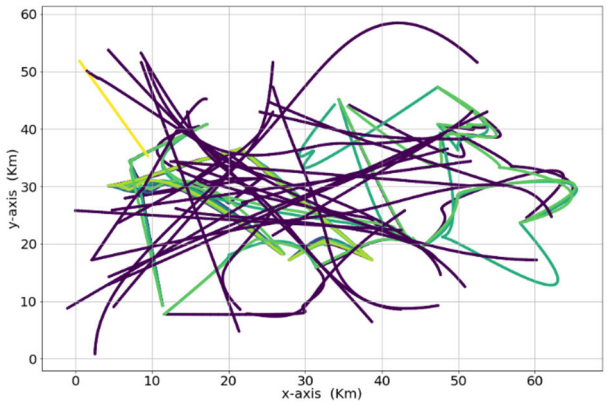

FIGURE 11. Scenario-1 DBSCAN results.

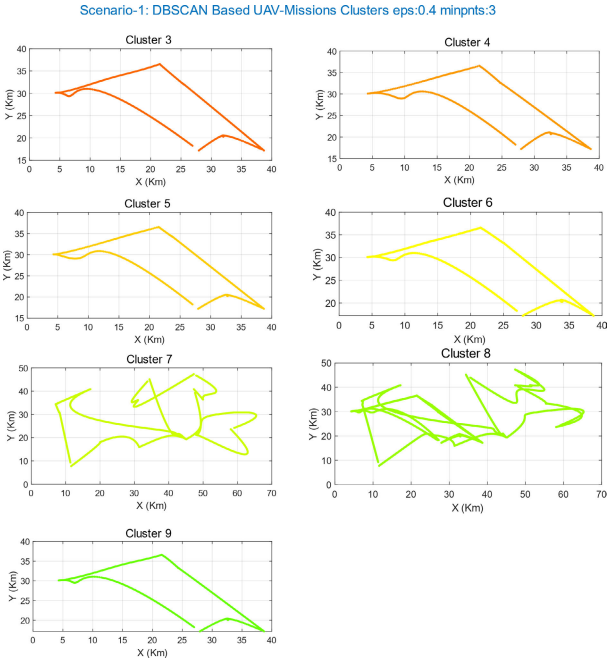

FIGURE 12. Scenario-1 DBSCAN detected mission cluster plots.

As observed, the presence of active static NFZs has clearly deviated the ideal straight line–based trapezoidal trajectories to a distorted shape for UAVs for COVID-19 samples. Also, the package delivery service UAV trajectories are much distorted from the ideal shapes for both UAV4 and UAV5 missions. The combined trajectory patterns, as depicted with the help of DBSCAN, are also shown in FIGURE 13.

We also evaluated the percentages of trajectory points per cluster for Scenario-1 as represented in FIGURE 14 below. It is evident that most of the trajectories detected belong to the COVID-19 sample delivery missions as shuttle service with 63% weight compared with delivery package services that constitute 37% of the detected missions.

3) SCENARIO 2—STATIC AIRFIELDS AND DYNAMIC RECREATIONAL AREAS WITH EXTREME WEATHER CONDITIONS

The detailed low-level clustered trajectory patterns detected with the above classifiers are shown in FIGURE 15 and

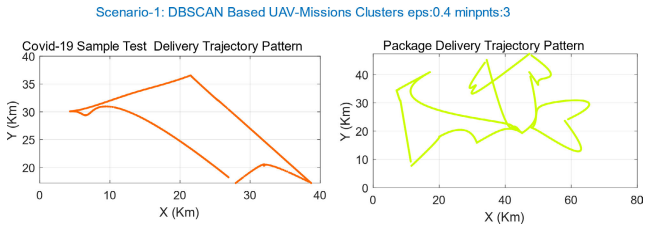

FIGURE 13. Scenario-1 detected combined mission patterns.

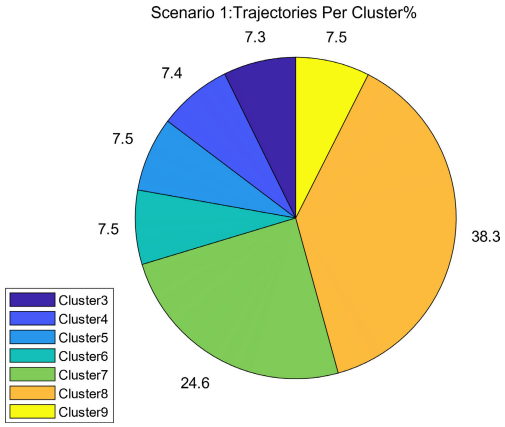

FIGURE 14. Scenario-1 trajectory count per cluster (%).

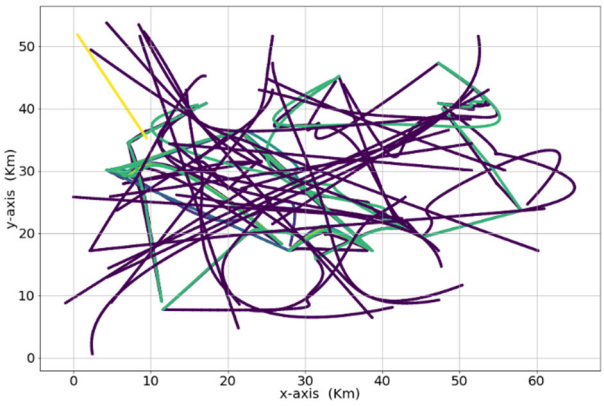

FIGURE 15. Scenario-2 DBSCAN results.

FIGURE 16. It can be observed from the separated cluster graphs that UAV1, UAV2, UAV3's COVID-19 shuttle service trajectory patterns are detected with a much higher confidence in clusters 3, 4, 5 and 7. UAV4 and UAV5's delivery package service trajectory pattern is only detected in cluster 6. Moreover, the presence of active static NFZs, dynamic obstacles and extreme weather conditions has clearly deviated the ideal trapezoidal trajectories to much more distorted shapes for the COVID-19 sample UAVs. Also, it can be seen that the delivery package service UAVs' trajectories are much distorted from the ideal straight line–legs and Scenario-1 for both UAV4 and UAV5 missions. The combined trajectory patterns depicted with the help of DBSCAN are also presented in FIGURE 17. The percentages of trajectory points per cluster for Scenario-2 as represented in FIGURE 18.

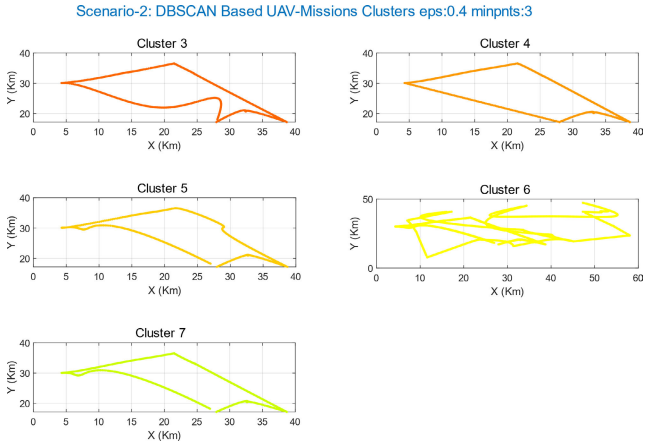

FIGURE 16. Scenario-2 DBSCAN detected mission cluster plots.

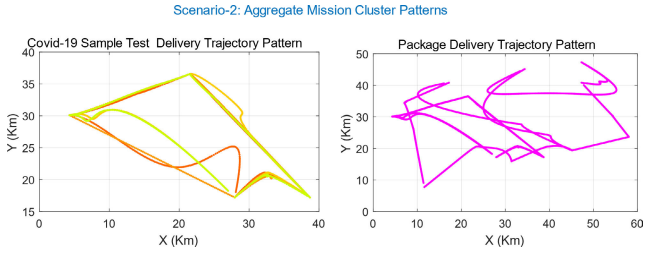

FIGURE 17. Scenario-2-detected combined mission patterns.

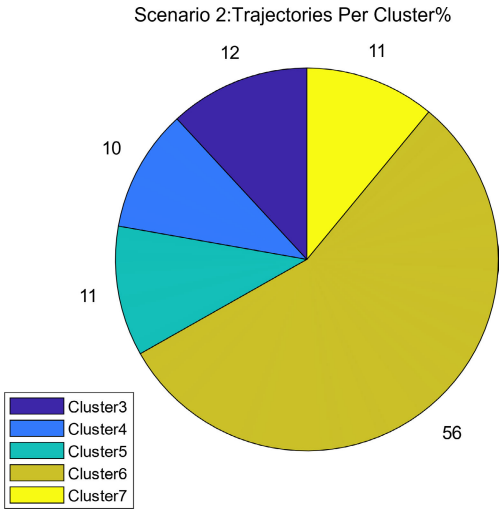

FIGURE 18. Scenario-2 trajectory count per cluster (%).

4) SCENARIO 3—DYNAMIC AIRFIELDS AND STATIC RECREATIONAL AREAS WITH DIFFERENT WEATHER CONDITIONS (RAIN AND WIND)

The detailed low-level clustered trajectory patterns detected with the above classifiers are shown in FIGURE 19 and FIGURE 20. It can be observed from the separated cluster graphs that COVID-19 shuttle service trajectory patterns (UAV1, UAV2, UAV3) are detected with a much higher confidence in clusters 3, 5, 6, 8 and 9. UAV4 and UAV5's delivery package service trajectory pattern is detected in

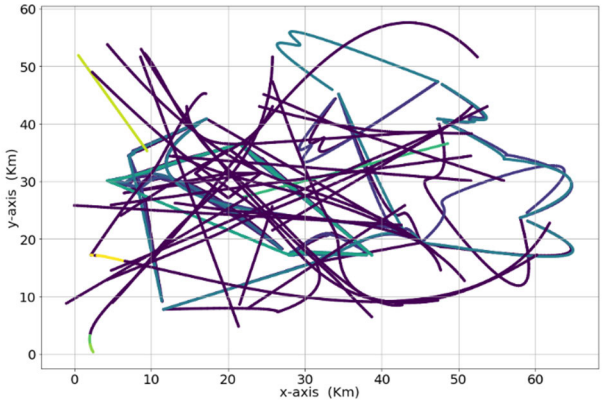

FIGURE 19. Scenario-3 DBSCAN results.

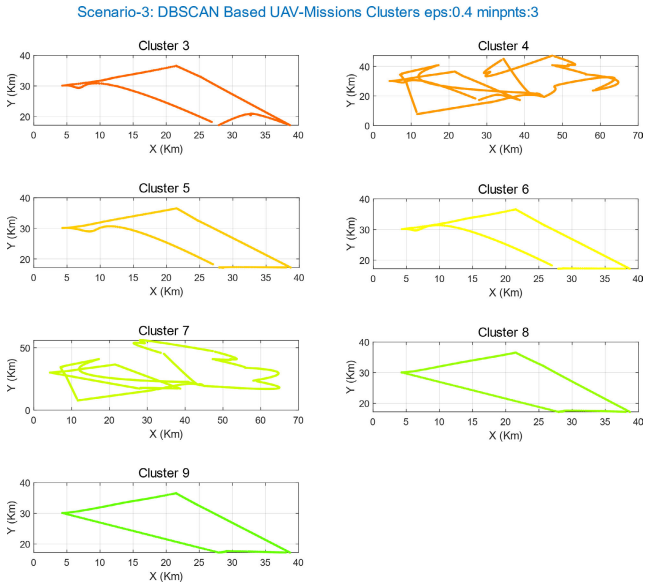

FIGURE 20. Scenario-3 DBSCAN detected mission cluster plots.

clusters 4 and 7. It can also be noted that presence of dynamic airfields, adverse winds and rain conditions has clearly deviated the ideal trapezoidal trajectories to much more distorted shapes for the UAVs carrying COVID-19 sample. Additionally, the delivery service UAVs' trajectories are severely distorted from the ideal straight line–legs, scenario-1 and scenario-2 for both UAV4 and UAV5 missions. The combined trajectory patterns depicted with the help of DBSCAN are also presented in FIGURE 21.

The percentages of trajectory points per cluster is represented in FIGURE 22.

B. STATISTICAL ANALYSIS OF CLUSTERS AND VALID TRAJECTORIES

The performance of DBSCAN-based mission clusters' detection is depicted in Table 5 below. The table presents the percentages of valid mission clusters and noisy clusters detected. As observed, under ideal weather conditions and no obstacles, DBSCAN detected more than 81% of valid mission clusters

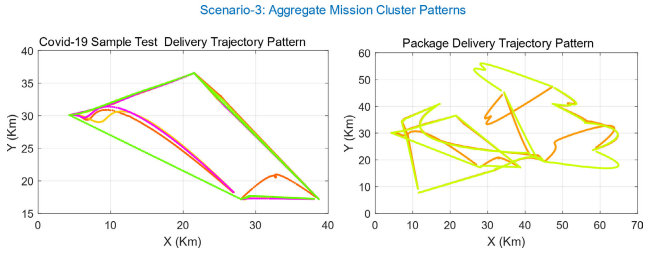

FIGURE 21. Scenario-3- detected combined mission patterns.

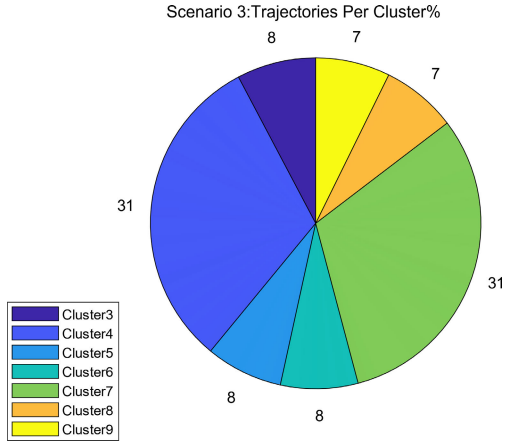

FIGURE 22. Scenario-3 trajectory count per cluster (%).

from the provided dataset. It is also observable that in the presence of static NFZs, the deviation in trajectory patterns reduced detection capability to almost 77%. These percentage levels have been further reduced to 71% in the presence of static airfields and dynamic recreational areas along with dynamic extreme weather clouds that passed by in almost all of the missions' execution areas at different times during the hour, heading between south-west and north-east. This percentage of valid clusters' detection has been reduced to almost 58% with dynamic airfields, static recreational areas, and weather conditions like wind and rain.

We also analyzed the number of valid missions detected from the overall cluster groups that should belong to subsets of COVID-19 sample delivery, package delivery and fire surveillance operation as presented in Table 6. Shuttle service–type missions were identified in large numbers as compared with one-time fire surveillance missions. This may be due to the reason that fire surveillance square loiter is missed in the detection mechanism because of the interference of much higher hobbyists' UAVs single-leg trajectories in this area. This also indicated the presence of much denser trajectories from diverse missions, dynamic environments, and random UAV flights in this area. The Gaussian density-based probability densities of this region may reflect the presence of congestion in this zone, which will be presented and discussed in Section C below.

C. UTM AIR TRAFFIC FLOW CHARACTERIZATION

This section presents a characterization of UTM air-traffic flows, with the help of the above mission clusters, as detected by DBSCAN. We will introduce three key characterization parameters (KCP), namely: Distance from Centroid (DFC), Distance To Complete Mission (DTCM), and Time To Complete Mission (TTCM). These parameters present the traffic-flow behavior and efficiency of the UTM airspace in three different scenarios, as explained in our simulation section. DFC is the measure of the horizontal deviation flows, whereas the DTCM and TTCM address the efficiency of UTM air traffic. These model parameters may facilitate the derivation of future configurations of UTM airspace structures. The concept of distance from centroid is inspired by several studies, as referenced below.

One recent article [83] uses the concept of convex polygon and centroid detection for UAV obstacle avoidance. In this study, the sensor carried by the UAV detects an obstacle, and the detected part is constructed with a convex polygon. The convex polygon with m vertices $(C_0, C_0)(C_1, C_1) \ldots, (x_{m-1}, y_{m-1})$ of the obstacle with centroid (C_x, C_y) is constructed, and a collision-avoidance cone is generated about this centroid to set the threshold angles for collision avoidance. The research in [84], in order to achieve better path planning of new areas to be covered during UAV search-and-coverage missions, uses the distance from centroid of uncovered portions of the boundary search region.

Lalak and Wierzbicki [85] use distance from centroid for detection and classification of aviation objects based on imagery data. In that study, Euclidean distance between the edges of an aviation object from its centroid is used to detect the geometry of the aviation object. For example, if this distance remains constant, this means a regular object shape is being detected, whereas if this distance varies, some irregular object (such as a polygon) is the subject.

Our work also employs this approach, and we measure the distances from the mission polygon centroid (DFC) to each point along the trajectory, in order to report deviations in missions along the whole trajectory. The concept of DFC measurement for shuttle-service missions and trajectory deviations is presented in FIGURE 23.

The centroids (C_x, C_y) are calculated using the area of mission polygon. The mission is represented by orange-colored contours. The black and green circles represent the maximum and minimum distances from centroids, namely, max_DFC and min_DFC, respectively. The DFC (x_1, y_1) and DFC (x_N, y_N) represent the distances from the centroid for trajectory points. We reported the maximum, minimum, mean and standard deviations in three different scenarios, in order to present the effects of dynamic obstacles, weather constraints and high-priority missions on these deviations. These factors indirectly affect efficiency, and they also highlight traffic-flow behaviors in UTM shuttle-service-based missions. Moreover, we were able to present a statistical analysis of DFC across different types of mission, to correlate and infer the type of shuttle-service missions that adversely affected traffic flow, and vice-versa.

Our work is inspired by the methods cited above, and we suggest distance from centroid (DFC) as one of the key

TABLE 5. Valid mission & noisy clusters' percentages.

Scenario	DBSCAN Parameters		Total Clusters	Valid Mission Clusters	Noisy Clusters	Valid Clusters %	Noisy Clusters %
	eps	minPts					
0	0.6	3	11	9	2	81.82	18.18
1	0.6	3	9	7	2	77.78	22.22
2	0.6	3	7	5	2	71.43	28.57
3	0.4	3	12	7	5	58.33	41.67

TABLE 6. Number & type of missions detected with DBSCAN.

Scenario	DBSCAN Parameters		Total Clusters	Mission Detected	Mission Patterns Detected		
	eps	minPts			Covid Samples Delivery	Royal Mail Package Delivery	Fire Surveillance
0	0.6	3	11	9	7	2	0
1	0.6	3	9	7	5	2	0
2	0.6	3	7	5	4	1	0
3	0.4	3	12	7	5	2	0

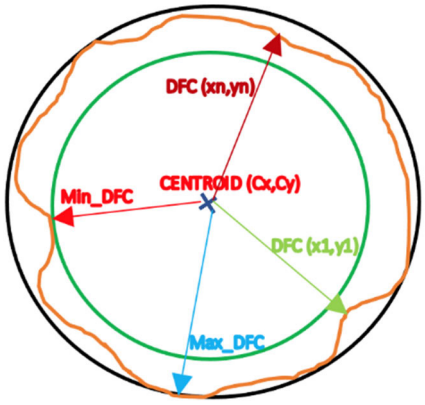

FIGURE 23. The concept of DFC measurement.

factors in understanding both UAV mission-path deviations and future capacity enhancements. This factor may form the basis of future efforts to ascertain traffic-flow behavior, especially for time-scheduled shuttle-service missions, and it plays a key role in dictating UTM traffic flows. This is the case, because shuttle-service missions of the same, or different, UAVs at a depot try to follow the same optimized planned trajectory in different time frames at margins of twenty minutes' delay, as simulated in our study. Nonetheless, the presence of dynamic obstacles, weather conditions and emergency operations prevent this, and deviations are forced that must then be evaluated by the UTM authority. Furthermore, it should be understood that the concept of traffic-flow behavior is slightly different from that of the ATC domain, as most urban-operation UAVs may operate in an airspace zone of 60 km x 60 km or less, without any terminal-maneuvering-area (TMA) requirements. This is especially true for vertical take-off and landing (VTOL) UAVs. Moreover, a number of the UAV missions are closed-loop scheduled missions, which do not evince any merging or leaving trends. This makes it necessary to model the deviation trends using DFC statistics.

Since both NHS Covid-19 sample delivery and the package-delivery service missions of UAVs form closed polygons, we used Euclidean distances from the centroid of this closed polygon (named Distance from Centroid (DFC)) as one of the modeling parameters. This was deployed for the UTM air-traffic-flow characterization of both the NHS and package-delivery service mission patterns detected, as described above, by DBSCAN.

The centroid is also known as the "center of gravity" or the "center of mass". This assumes the polygon is closed, so that the last point position (x_N, y_N) is the same as the first (x_1, y_1), where N is the number of points in the mission trajectory set, or in mathematical-shape terms, the number of vertices in the polygon. The x and y co-ordinates of this centroid (C_x, C_y), for a polygon of this kind, are governed by the following set of equations [83], [86]:

$$C_x = \frac{1}{6A}\sum_{i=0}^{N-1}(x_i + x_{i+1})\,(x_i y_{i+1} - x_{i+1} y_i) \tag{9}$$

$$C_y = \frac{1}{6A}\sum_{i=0}^{N-1}(y_i + y_{i+1})(x_i y_{i+1} - x_{i+1} y_i) \tag{10}$$

where x and y are the co-ordinates of our trajectory $T(x, y)$. A is the area of the mission polygon. The polygon is comprised of line segments between N vertices (x_i, y_i), $i = 1$ to N. The position of the last vertex (x_N, y_N) is assumed to be the same as the first (i.e., the polygon is closed). Subsequently,

the area of this closed polygon is calculated using the following equation:

$$A = \frac{1}{2}\sum_{i=0}^{N-1}(x_i y_{i+1} - x_{i+1} y_i) \tag{11}$$

In this study, we used the built-in function centroid in MATLAB to calculate the centroids of our mission polygons. The Distance from Centroid (DFC) is a Euclidean distance between the centroid of the mission polygon and current trajectory point $T(x, y)$, as shown in the equation below:

$$ADFC\left(C_m, T_j\right) = \sqrt{\left(C_{mx} - x_j\right)^2 + \left(C_{my} - y_j\right)^2} \tag{12}$$

where C_m is the centroid for any mission (m), and C_{mx}, C_{my} represents the x, y co-ordinates of the centroid. The T_j represents the j^{th} point of the trajectory, with (x_j, x_j), co-ordinates.

Once the centroid was known, we calculated the Euclidean distance between this centroid C_x, C_y for each point in the mission trajectory (DFC). This was done to analyze the deviation trends, using the statistical measures of mean, max, min and standard deviation (mean_DFC, max_DFC, min_DFC, std_DFC) for each mission detected by DBSCAN.

Furthermore, in order to characterize the traffic-flow behavior based on distance to go, we also computed the Distance To Complete Mission (DTCM) that each UAV mission traversed; this was because ideal planned distance might differ from the real planned distance in the presence of the aforementioned constraints. This was followed by the calculation of the Time To Complete Mission (TTCM), using a constant UAV speed (Uv) of 90 km/hr. The mathematical representation of these two parameters is presented below:

$$DTCM = \|T_i - T_{i+1}\|_2 = \sqrt{\sum_{i=0}^{n-1}(x_i - x_{i+1})^2 + (y_i - y_{i+1})^2} \tag{13}$$

where n is the number of trajectory points in the mission.

$$TCM = \frac{DTCM}{Uv} \tag{14}$$

The above parameters were measured and presented for three simulation scenarios, along with the ideal scenario-0; and in this way, we considered the ideal weather conditions and absence of no-fly zones.

1) UTM TRAFFIC FLOW CHARACTERIZATION—SCENARIO-0

This section includes the results and discussion concerning the KCPs (DFC, DTCM and TTCM) for the ideal case scenario, *with* normal weather conditions, and *without* NFZ restrictions.

a: DISTANCE FROM CENTROID (DFC)

The detected mission polygons with centroids for both NHS Covid-19 sample delivery and commercial package-delivery services are presented in FIGURE 24. Next, we present

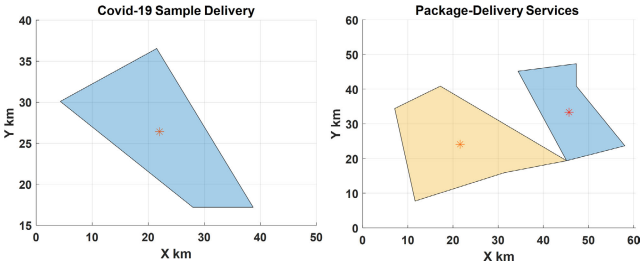

FIGURE 24. Scenario-0: Covid-19 sample delivery (left) and delivery services (right) mission polygons with centroids (*).

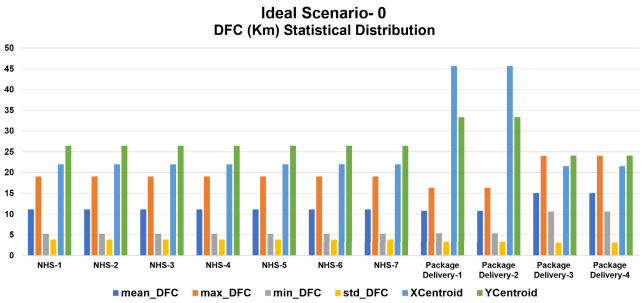

FIGURE 25. Scenario-0: NHS and delivery services (DS) missions DFC statistical distribution.

the statistical distribution of DFC for all these missions by analyzing the mean, maxima, minima and standard deviations for the DFC curves. In addition, this analysis evaluates the deviations of the above factors, along with the deviation of centroids for each detected mission for NHS Covid-19 sample delivery (NHS) and the package-delivery services (DS). The results are presented graphically in FIGURE 25.

It is clear that in the ideal case scenario, UTM traffic-flow patterns, as identified by DBSCAN, exhibited zero deviation of DFC values for all the high priority NHS Covid-19 sample-delivery missions, as well as the commercial (Royal Mail) delivery services. Thus, a clear, sunny day, without any NFZ constraints, exhibits a zero deviation in mean, max, min and standard deviations for DFC. Furthermore, the (x, y) centroids of the described missions retained their constant positions in this scenario. This means that every group of shuttle-service missions followed the same path, without any deviations.

b: DISTANCE TO COMPLETE MISSION (DTCM) AND TIME TO COMPLETE MISSION (TTCM)

This section provides the DTCM and TTCM analysis for the ideal case scenario, whereby the DTCM and TTCM metrics are calculated using (13) and (14). A constant UAV speed of 90 km/hr is assumed in these calculations. FIGURE 26 demonstrates that zero deviation in DTCM and TTCM values was observed for all the high-priority NHS Covid-19 sample-delivery missions, and also for the commercial-delivery services, in the case of moderate weather without any NFZ constraints.

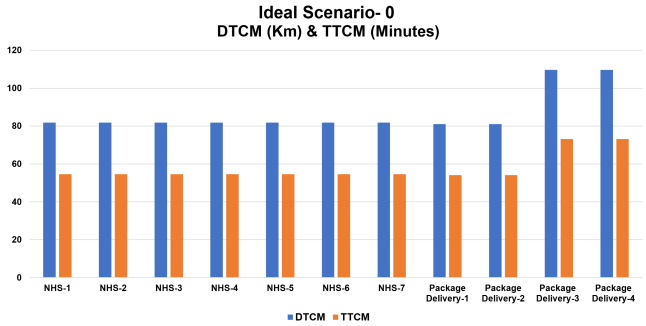

FIGURE 26. DTCM & TTCM distribution for Scenario-0.

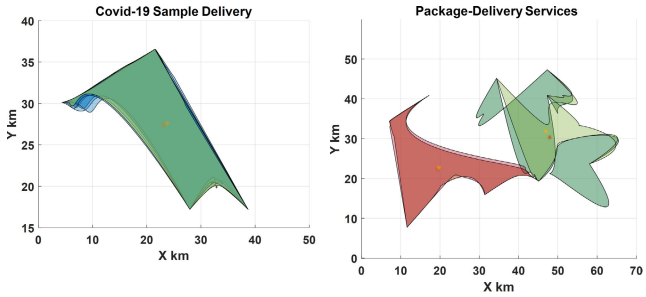

FIGURE 27. Scenario-1: Covid-19 sample delivery (left) and delivery services (right) mission polygons with centroids (*).

2) UTM TRAFFIC FLOW CHARACTERIZATION—SCENARIO-1

This section includes the results and discussion regarding the KCP (DFC, DTCM and TTCM) for Scenario-1, whereby the Bedfordshire area was assumed to have an active static NFZ, without any dynamic obstacles or weather constraints.

a: DISTANCE FROM CENTROID (DFC)

The detected mission polygons with centroids for NHS Covid-19 sample delivery and the package-delivery services are presented below, in FIGURE 27. Next, we present the statistical distribution of DFC for all these missions, by analyzing the mean, maxima, minima and standard deviations for DFC curves. This analysis also assesses the deviations of the above factors for a group of hourly shuttle-service missions. The NHS-1 to NHS-7 shuttle services belong to one group, whereas DS1 and DS2 belong to another group, and DS3, DS4 constitute the same group. We also measured the deviations of centroids for each detected mission. The statistical distribution is presented graphically in FIGURE 28.

It is evident, from the analysis above, that in the case of Scenario-1, traffic-flow patterns show deviations in DFC values for all the high-priority NHS Covid-19 sample-delivery missions, as well as for the commercial-delivery services. The range of deviations in mean, maxima, minima and standard deviations for the DFC curves in this case are as follows. The mean DFC varies between 0.04 km and 1.6 km; the maximum DFC varies between 0.01 km and 4.35 km; the minimum values lie between 0.05 km and 1.14 km; and the standard deviation varies between 0.002 km and 1.16 km. In addition to this spread, a shift is also observed in centroid positions.

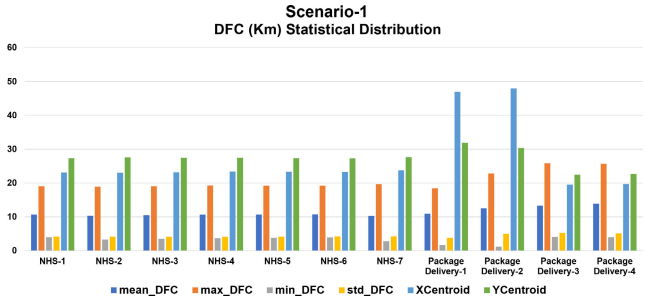

FIGURE 28. Scenario-1: NHS and DS missions DFC statistical distribution.

Specifically, the X centroid varies between 0.03km and 0.96 km, and the Y centroid shifts between 0.02 km and 1.55 km. This means that the NHS and the delivery shuttle-service missions changed their routes in both X,Y planes, and they also increased their spread from the mission polygon centroid by a maximum distance of approximately 4.3 km.

b: DISTANCE TO COMPLETE MISSION (DTCM) AND TIME TO COMPLETE MISSION (TTCM)

This section provides the DTCM and TTCM analysis for the case Scenario-1. The characterization parameters are presented using a stacked bar chart, as shown below in FIGURE 29.

We also observed deviations in the DTCM and TTCM for each group of the shuttle-service missions belonging to the NHS emergency services and commercial services. This analysis demonstrated that, in the presence of static NFZ in the Bedfordshire area, there was some significant deviation of DTCM and TTCM values. For example, the DTCM for the hourly NHS shuttle services varied between 0.3 km and 1.54 km, whereas the DTCM variations for the hourly delivery services shuttle missions ranged between 0.4 km and 20.98 km. The TTCM for the NHS missions varied between 0.24 minutes and 1 minute. The commercial delivery shuttle services exhibited an increase in their mission times from 0.27 minutes to 13.98 minutes.

3) UTM TRAFFIC FLOW CHARACTERIZATION—SCENARIO-2

This section presents the results and discussion regarding the three KCP for Scenario-2. Here, the Bedfordshire area has static airfields and dynamic recreational areas, with extreme weather conditions.

a: DISTANCE FROM CENTROID (DFC)

The detected mission polygons with centroids for our scenario missions are presented below, in FIGURE 30. Similarly, we present the statistical distribution of DFC for all these missions by analyzing the mean, maxima, minima and standard deviations for DFC curves. The statistical distribution is presented graphically in FIGURE 31.

The analysis demonstrates that, in the case of Scenario-2, traffic-flow patterns evince significant deviations in DFC values for both high priority NHS Covid-19 sample-delivery

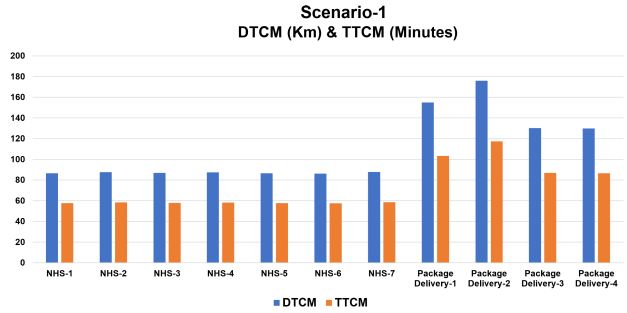

FIGURE 29. DTCM & TTCM distribution for Scenario-1.

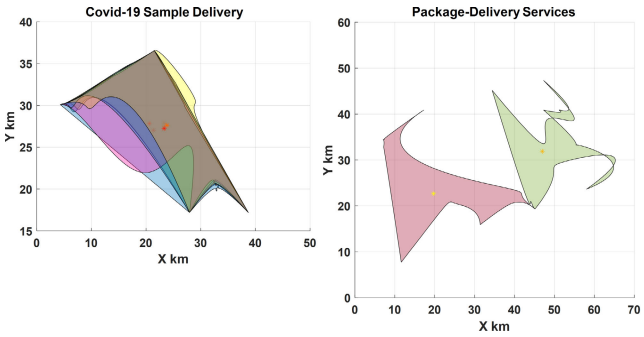

FIGURE 30. Scenario-2: Covid-19 sample delivery (left) and delivery services (right) mission polygons with Centroids (*).

missions and delivery services. The mean_DFC varies between 0.06 km and 1.19 km; meanwhile, the maximum DFC varies between 0.05 km and 2.059 km, the minimum values lie between 0.128 km and 6.38 km, and the standard deviation varies between 0.005 km and 1.97 km. In addition to this spread, a large shift in centroid positions is also observed; the X centroid varies between 0.108km and 1.88 km, and the Y centroid shifts between 0.2 km and 1.44 km. This means that NHS and the delivery shuttle-service missions not only changed their routes in both X, Y planes, but they also shifted their polygon centroids with reference to the ideal case scenario.

b: DISTANCE TO COMPLETE MISSION (DTCM) AND TIME TO COMPLETE MISSION (TTCM)

As indicated in FIGURE 32, deviations can be observed in DTCM and TTCM values for each group of shuttle service, for static recreational areas, dynamic airfields and extreme weather fronts in the Bedfordshire area. The DTCM values for hourly NHS shuttle services varied between 0.82 km and 8.5 km, whereas the DTCM variations for the hourly delivery shuttle-service missions ranged between 20 km to 73 km, when we compared results with ideal case Scenario-0. The TTCM for NHS missions ranged between 0.54 minutes and 5.67 minutes. The package-delivery services missions registered an increase in mission-completion times between 13 minutes and 49 minutes, with reference to ideal case Scenario-0. This clearly shows that the extreme weather fronts, along with the dynamic recreational-area constraints,

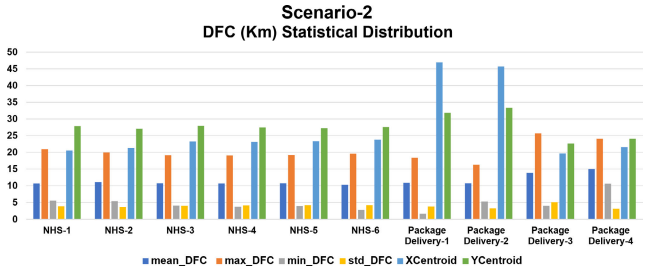

FIGURE 31. Scenario-2: NHS and DS missions DFC statistical distribution.

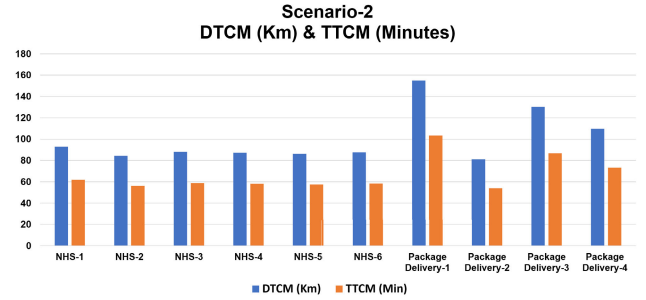

FIGURE 32. DTCM & TTCM distribution for Scenario-2.

resulted in elongated mission distances and times, and these factors thus require attention from UTM authorities.

4) UTM TRAFFIC FLOW CHARACTERIZATION—SCENARIO-3

This section presents the results and discussion concerning the three KCP for Scenario-3, whereby the Bedfordshire area has dynamic airfields and static recreational areas, with ''rainy and windy'' weather conditions.

a: DISTANCE FROM CENTROID (DFC)

The detected mission polygons with centroids, for our scenario missions, are presented in FIGURE 33, and the statistical distribution is presented graphically in FIGURE 34.

It can be seen from the above analysis that, in the case of Scenario-3, traffic-flow patterns evince significant deviations in DFC values. The mean_DFC varies between 0.014 km and 3.20 km, whereas the maximum DFC varies between 0.016 km and 8.6 km, the minimum values range between 0.06 km and 1.62 km, and the standard deviation varies between 0.053 km and 2.593 km. In addition to this spread, a large shift is also observed in centroid positions; the X centroid varies between 0.0.4km and 1.709 km, and the Y centroid shifts between 0.008 km and 1.035 km. This means that NHS and the package-delivery services missions not only change their routes in both X,Y planes; they also shift their centroids.

b: DISTANCE TO COMPLETE MISSION (DTCM) AND TIME TO COMPLETE MISSION (TTCM)

As FIGURE 35 indicates, more deviations are observed in DTCM and TTCM values for each group of NHS and package-delivery services, due to the constraints imposed by dynamic recreational areas, static airfields and adverse

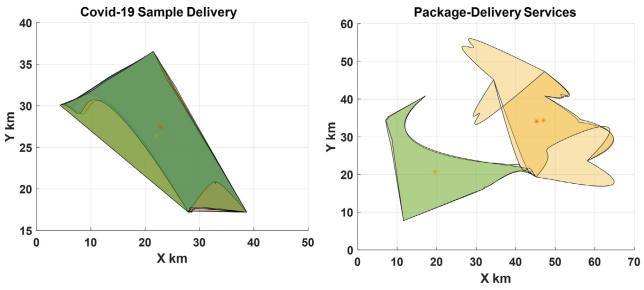

FIGURE 33. Scenario-3: Covid-19 sample delivery (left) and delivery services (right) mission polygons with centroids (*).

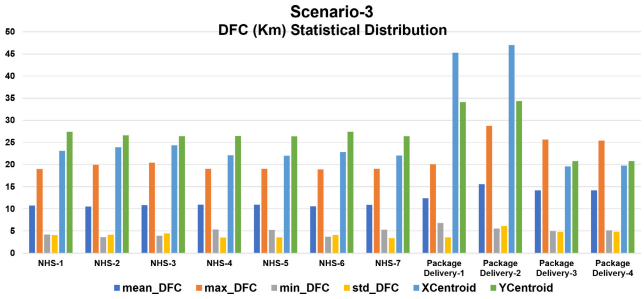

FIGURE 34. Scenario-3: NHS and DS missions DFC statistical distribution.

weather conditions, such as rain and wind in the Bedfordshire area.

The DTCM values for hourly NHS shuttle services vary between 0.05 km and 4.99 km. The DTCM variations for hourly delivery shuttle-service missions, meanwhile, range between 0.47 km and 6.91 km. TTCM for NHS missions varies between 0.038 minutes and 3.32 minutes. The delivery services missions evinced an increase in mission-completion times from 0.317 minutes to 4.60 minutes. This shows that rainy and windy conditions, along with NFZ constraints, also resulted in extended mission distances and times, and these variables will be affected by the efficiency of airspace.

D. UTM AIRSPACE CONGESTION ANALYSIS USING GAUSSIAN KERNEL DENSITY ESTIMATOR (KDE)

The authors will, in this section, estimate airspace density for the Bedfordshire area. The aim of this analysis is to locate the regions or zones of higher density or congestion that may reflect the safety and availability of UTM airspace. The traffic density, which is defined as the amount of aircraft traversing a particular sector, is a conventional metric of air traffic complexity [87]. The density of UAVs' trajectories in an available region has been estimated by analyzing the whole airspace. All scenarios discussed previously have been utilized for the purpose of evaluating the UTM airspace density on the spatial scale. High to low density of UAVs is denoted by yellow to violet colors that mark more populated areas and less populated areas, respectively.

During severe weather disorders along with emergency operations conducted through UAVs, the UTM operator is responsible for ensuring the safety of flight operations. In the

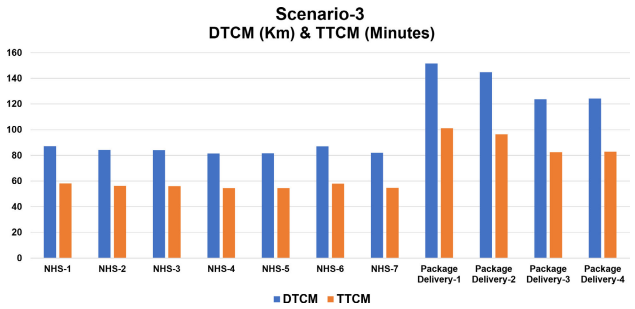

FIGURE 35. DTCM & TTCM distribution for Scenario-3.

above regard, UTM service providers also judge the capacity of the airspace in order to determine the availability of alternate routes for smooth UTM traffic flow. One of the examples is the diversion of flight movements to off-peak times or suggesting alternate nearby airports/depots with less congestion or diversion to less congested traffic segments.

The visualize and predict the congestion will help the UTM operator to divert the less priority UAV missions such as recreational UAV flyers to lesser congested areas, in order to regulate the traffic flow and significantly reduce the congestion in the airspace, also offering more availability to upcoming high priority UAV missions. This may help the UTM authority to better manage the airspace safety and availability under real conditions.

The analysis of the data conducted in this study facilitates risk analysis and enhances the planning of trajectories in various aircraft zones taking into account each dynamic parameter that could result in aircraft deviating from their normal trajectory. These findings enable cross-route comparisons of the efficiency of the traffic flow in varying flight situations, in addition to the determination of the factors causing aircraft deviations from their standard routes. Moreover, the airspace density pinpoints some ideal regions to conduct UAV operations that minimizes the impact on conventional ATM.

Information pertaining to the flow and performance of traffic sourced from the analysis of trajectory data can lay the foundation for the development of innovative approaches, processes and tools for supporting decisions in the field of air traffic management. For example, this innovation spans from developing an artificial intelligent architecture capable of predicting airspace congestion patterns to classifying safe and dangerous regions using historic UAVs traffic patterns.

In our work, airspace density has been evaluated using the Gaussian Kernel Density Estimator. KDE is frequently employed in the field of computer vision for identifying target objects as in [88]. Additionally, it is utilized for the visualization and analysis of spatial data, with the aim of forecasting event trends [89]. It is also widely applied in areas such as analyzing damage and assessing risk [90]. KDE is also applied in the transportation field. Laxhammar et al. utilized KDE for the purpose of identifying abnormalities in marine traffic [91].

We used both x and y data pairs as the dataset fed to Kernel Density Estimation (KDE). KDE is a non-parametric

technique utilized for the estimation of data distribution according to a finite sample dataset with no presumptive distributional properties [92]. It is well understood that out of different probability density functions, (pdf) optimally demonstrates how the 100% probability mass is distributed across the values of a random variable, X. The traditional empirical representation of pdf, namely the histogram, is significantly subjective due to the fact that it is dependent on the subjective selection of the amount (or widths) of class intervals (bins) to which the sample range is then divided, as well as the selection of the starting point. These limitations do not apply to the kernel estimation of probability density function. When applied practically, it largely generates a smooth empirical pdf according to specific locations of the entire sample data.

We computed the KDE based PDF for our bivariate trajectory data (x, y) using the gaussian_KDE () function in python. This function automatically determines the estimator bandwidth using Scotts Rule as the default parameter. We then used the computed PDF for providing congestion contours representing the congestion percentages (%) by normalizing the PDF data between 0 and 100. The original PDF lies between 0-1 and represents the per unit increase in kilometers of bivariate data of two trajectory variables x and y. This percentage congestion is plotted as contour maps for the whole span of spatial trajectory data. The results and discussion for KDE and % congestion contours are provided below for each simulation scenario.

A KDE estimation graph for Scenario-1 of UAV missions with static NFZs, no weather constraints and no dynamical obstacles for the first hour (9:00 am to 10:00) is presented in FIGURE 36.

It has been observed that static areas (NFZs) also exert some impact on the UAV trajectories, resulting in large deviations that cause congestion in different regions of the UTM airspace over Bedfordshire. The regions of Dunstable, Sandy, Cardington and Graveley evince lower regional congestion, as compared with others. It is also observed from percentage congestion contour plots that some areas near Milton Keynes prison present more than 80% congestion levels. This is a result of local emergency firefighting operations. This observation suggests the need to regulate the traffic flow in these congested UTM traffic-flow zones.

A KDE estimation graph for Scenario-2 of UAV missions with static airfields and dynamic recreational areas with extreme weather conditions for the second hour (10:00 am to 11:00), is presented in FIGURE 37. These dynamics are sporadic, with some regions available and others unavailable throughout the hour.

In this scenario, it has been observed that the density is increased due to a large variation in dynamic and static areas during the hour. Dynamic extreme weather conditions also play an important role in increasing the density of UAV trajectories in some areas as their trajectories deviates to avoid static NFZs and weather fronts. Due to extreme weather constraints, maximum UAVs trajectories confined themselves to

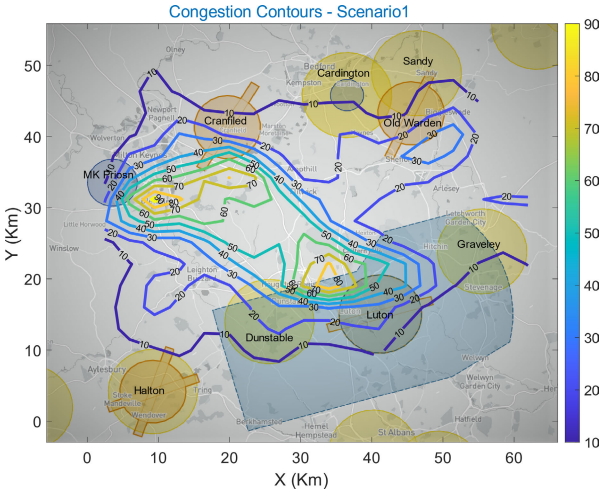

FIGURE 36. Airspace congestion identification for scenario1.

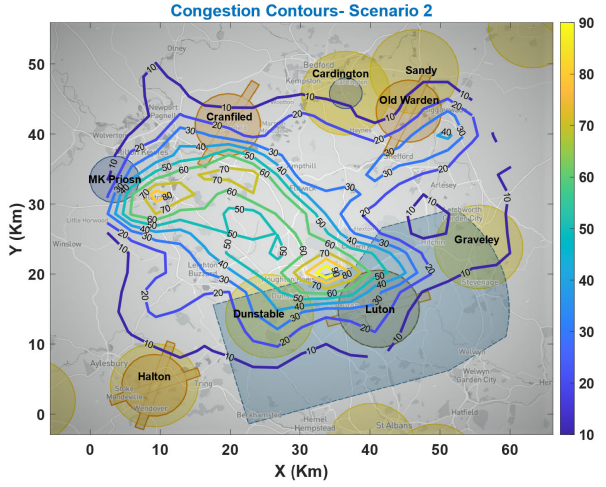

FIGURE 37. Airspace congestion identification for scenario 2.

a limited area in the whole airspace, as represented by the yellow and green colors in FIGURE 37. It is observed from congestion contour plots that some areas near Milton Keynes and Luton experience more than 80% congestion levels.

KDE analysis for the third hour of data simulation with dynamic airfields, static recreational areas and different weather conditions (rain and wind) is presented in FIGURE 38.

It is observed from congestion contour plots that some areas near Milton Keynes, Luton and Dunstable experience more than 70% congestion levels. There is also an observation of about more than 50% congestion levels in some parts of north-west and south-west of Bedfordshire area and thus UTM traffic flow may be regulated in these zones. It is thus inferred that regions in the north- west and south-east are more prone to hazards and conflicts, as both areas saw maximum UAV-trajectory congestion exceeding 50%, reaching a maximum of 90% congestion levels for some smaller areas. The reason for the lower congestion of the north-east and south-west regions, conversely, is that they

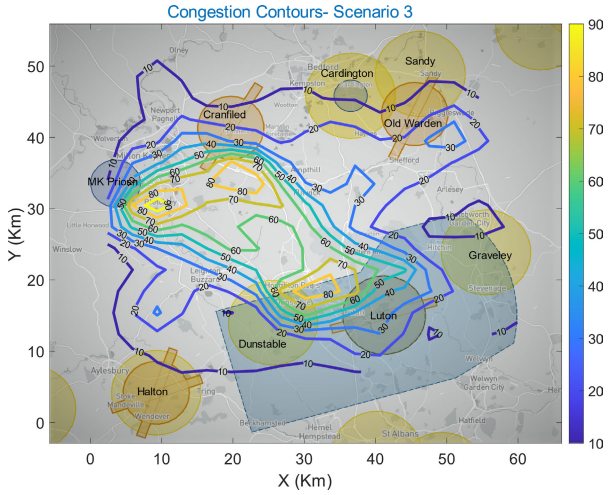

FIGURE 38. Airspace congestion identification for scenario 3.

are generally occupied by static and dynamic NFZs with extreme weather constraints; therefore, most UAVs keep their trajectory points away from these regions, avoiding NFZs and extreme weather, leading to more UAV congestions in the remaining airspace regions. This also explains why only the fire-surveillance missions by UAV-6 fail to be detected by the DBSCAN algorithm, as this is considered a noisy pattern and is thus lost in this congested area. The temporal weather effect shows that extreme weather fronts and adverse wind and rain cause some local hotspots, with congestion levels more than 90% as compared to normal weather conditions.

VI. CONCLUSION AND FUTURE WORK

This work has proposed and implemented a framework for UTM traffic flow's spatial and spatiotemporal patterns identification and characterization using DBSCAN clustering algorithm. Moreover, this work has analyzed the airspace density using the Gaussian kernel density estimator (KDE) for different UAV missions under variable airspace structures and environmental factors. UAV missions considered in this study as an application use case are essential delivery services for COVID-19 samples, package delivery services and emergency fire surveillance tasks. This work also considers the influence of random flights of UAV hobbyists or recreational users during the execution of above essential missions. The effect of airspace structure configurations like static NFZs, dynamic airfields, recreational areas and environmental factors such as weather conditions including wind, rain and extreme weather have also been incorporated and studied in this work.

It has been observed that the unsupervised learning algorithm DBSCAN can detect and identify 82% of UAV missions under ideal weather conditions and in absence of flying restrictions. The valid missions' detection capability of DBSCAN is reduced by 4% under NFZ restrictions and by 10% in the ideal scenario with static airfields, dynamic recreational area restrictions and extreme weather fronts. This performance is further deteriorated by almost 23% with static recreational areas, dynamic airfields and bad weather conditions including wind and rain. The noisy clusters incorporate almost all single-leg trajectories belonging to recreational users.

It has been observed that types of mission such as COVID-19 sample delivery and package delivery that run as shuttle services were identified in large numbers as compared with the one-time fire surveillance mission because this mission is in the region of maximum interference or congestion, and there is a greater concentration of random trajectories of hobbyists' UAVs as presented in the KDE-based density graphs. This phenomenon resulted in the declaration of such a square polygon as an outlier cluster pattern.

It is also evident from the detected mission-cluster patterns that the ideal trapezoid trajectory polygon shapes, as expected in ideal case Scenario-0 (FIGURE 8 and FIGURE 9, are changed and deformed (FIGURE 13, FIGURE 17 and FIGURE 21), showing the presence of NFZs, obstacles and weather constraints. The packages-delivery-mission patterns seem most affected; these show far more diversions and present ''flower-petal'' shapes, as compared with the ideal Scenario-0. The reason for this is that this mission is obliged to provide emergency services, when NFZs and dynamic obstacles are present along with the worst weather conditions.

It can also be concluded from the UTM mission characterization that severe weather conditions and dynamic NFZ are the key sources of UTM-mission unpredictability in the Bedfordshire area. It is observed that UTM missions disperse more in the airspace, with a maximum spread of about 8.6 km. Furthermore, there appears to be a shift in the mission centroids by a maximum margin of 1.88 km in horizontal directions, and of 1.55km in a southerly direction. Indeed, there seems to be increased shifting of missions in the horizontal directions. The commercial package-delivery services are subject to stronger adverse effects, in comparison with the emergency NHS Covid-19 sample-delivery services. Moreover, the mission ranges increased drastically, by 20 km to 79 km in the worst cases, as compared with ideal weather conditions without any NFZ restrictions. Similarly, the mission-completion times also increased by an order of 14 to 49 minutes in the worst-case scenarios.

For a better congestion analysis using KDE, the percentage congestion contours are evaluated to provide better suggestions for UTM operator as visual data analytics to regulate better traffic flow based on congestion figures. The hot zones with more than 80% congestion levels in Bedfordshire area are pinpointed in this study using the above approach. It is inferred from the KDE analysis that the north-west and south-east regions are more congested, as compared with other regions of Bedfordshire airspace. The DBSCAN clustering algorithm thus detects UAV trajectory patterns where there is less congestion as compared with densely packed trajectory zones due to random single-leg missions of UAV-flying hobbyists. It is hence concluded that congested

areas depict conflicts and concerns related to the safety of the airspace.

It is thus inferred that clustering algorithms can be good candidates in classifying and detecting up to 82% of the UAV mission trajectories, and these statistics reduce to about 58% in the worst-case scenarios. The performance of detection is deteriorated due to the presence of noisy trajectory patterns belonging to random UAV flights of hobbyists, dynamic airspace structure and weather constraints. Moreover, Gaussian kernel density-based estimators may help in evaluating the congestion in the airspace

This future work under progress mentioned above concerns designing and developing an AI (artificial intelligence)-based architecture capable of predicting airspace congestion patterns and classifying safe and dangerous regions using historic traffic patterns of UAVs. Moreover, we are considering the application of the above work regarding UTM airspace patterns' identification and congestion measurement for some other UK airspace regions that have a more diverse set of airspace configurations and expect a much denser UAV traffic flow. We are also proposing to design more realistic and complex operational scenarios in future works. The knowledge derived from the above studies regarding traffic flows and their performance analysis can form the basis to design and develop new approaches, practices, and decision support tools for better air traffic management.

REFERENCES

[1] P. Sul'aj, R. Haluska, L. Ovsenik, S. Marchevsky, P. Pulli, and V. Kramar, "UAV management system for the smart city," in *Proc. World Symp. Digit. Intell. Syst. Mach. (DISA)*, Aug. 2018, pp. 119–124, doi: 10.1109/DISA.2018.8490535.

[2] A. Carrio, C. Sampedro, A. Rodriguez-Ramos, and P. Campoy, "A review of deep learning methods and applications for unmanned aerial vehicles," *J. Sensors*, vol. 2017, pp. 1–13, Jun. 2017, doi: 10.1155/2017/3296874.

[3] M. Radmanesh, M. Kumar, A. Nemati, and M. Sarim, "Dynamic optimal UAV trajectory planning in the national airspace system via mixed integer linear programming," *Proc. Inst. Mech. Eng. G, J. Aerosp. Eng.*, vol. 230, no. 9, pp. 1668–1682, Jul. 2016, doi: 10.1177/0954410015609361.

[4] P. Kopardekar, "Enabling civilian low-altitude airspace and Unmanned Aerial System (UAS) operations by unmanned aerial system traffic management (UTM)," *AUVSI Unmanned Syst.*, vol. 2, pp. 1678–1683, Apr. 2014.

[5] W. Schuster, "Trajectory prediction for future air traffic management–complex manoeuvres and taxiing," *Aeronaut. J.*, vol. 119, no. 1212, pp. 121–143, Feb. 2015, doi: 10.1017/S0001924000010307.

[6] ICAO. *Unmanned Aircraft Systems Traffic Management (UTM)—A Common Framework With Core Principles for Global Harmonization*. UTM Guid. Accessed: 2019. [Online]. Available: https://www.icao.int/safety/UA/Documents/UTM-Framework.en.alltext.pdf

[7] B. M. Albaker and N. A. Rahim, "A conceptual framework and a review of conflict sensing, detection, awareness and escape maneuvering methods for UAVs," in *Aeronautics and Astronautics*. Rijeka, Croatia: InTech, 2011, pp. 550–570, doi: 10.5772/26567.

[8] S. Zsolt, "Unmanned peer-reviewed article model of the system of information for the traffic management of unmanned," *J. UNMANNED Aer. Syst. Introd.*, vol. 4, no. 1, pp. 18–31, 2019.

[9] *Enabling Civilian Low-Altitude Airspace and Unmanned Aerial System (UAS) Operations*, NASA Ames Res. Center, Moffett Field, CA, USA, 2014, pp. 1–18.

[10] M. C. R. Murça, M. X. Guterres, M. de Oliveira, J. B. T. Szenczuk, and W. S. S. Souza, "Characterizing the Brazilian airspace structure and air traffic performance via trajectory data analytics," *J. Air Transp. Manage.*, vol. 85, Jun. 2020, Art. no. 101798, doi: 10.1016/j.jairtraman.2020.101798.

[11] X. Oliver, L. Basora, B. Viry, R. Alligier, X. Olive, and B. Viry, "Deep trajectory clustering with autoencoders," in *Proc. ICRAT*, 2020, pp. 1–8, [Online]. Available: https://hal-enac.archives-ouvertes.fr/hal-02916241

[12] X. Olive and L. Basora, "Detection and identification of significant events in historical aircraft trajectory data," *Transp. Res. C, Emerg. Technol.*, vol. 119, Oct. 2020, Art. no. 102737, doi: 10.1016/j.trc.2020.102737.

[13] Z. Sándor, "Challenges caused by the unmanned aerial vehicle in the air traffic management," *Periodica Polytechnica Transp. Eng.*, vol. 47, no. 2, pp. 96–105, Dec. 2017, doi: 10.3311/PPtr.11204.

[14] S. Bijjahalli, R. Sabatini, and A. Gardi, "Advances in intelligent and autonomous navigation systems for small UAS," *Prog. Aerosp. Sci.*, vol. 115, May 2020, Art. no. 100617, doi: 10.1016/j.paerosci.2020.100617.

[15] Z. Feng and Y. Zhu, "A survey on trajectory data mining: Techniques and applications," *IEEE Access*, vol. 4, pp. 2056–2067, 2017, doi: 10.1109/ACCESS.2016.2553681.

[16] D. Wang, T. Miwa, and T. Morikawa, "Big trajectory data mining: A survey of methods, applications, and services," *Sensors*, vol. 20, no. 16, p. 4571, Aug. 2020, doi: 10.3390/s20164571.

[17] Y. Zheng, "Trajectory data mining: An overview," *ACM Trans. Intell. Syst. Technol.*, vol. 6, no. 3, pp. 1–41, 2015, doi: 10.1145/2743025.

[18] G. Antonini and J. P. Thiran, "Counting pedestrians in video sequences using trajectory clustering," *IEEE Trans. Circuits Syst. Video Technol.*, vol. 16, no. 8, pp. 1008–1020, Aug. 2006, doi: 10.1109/TCSVT.2006.879118.

[19] J. Ackley, T. G. Puranik, and D. N. Mavris, "A supervised learning approach for safety event precursor identification in commercial aviation," in *Proc. AIAA Aviat. Forum*, vol. 1, Jun. 2020, p. 2880, doi: 10.2514/6.2020-2880.

[20] D. R. De Almeida, C. D. S. Baptista, and F. G. De Andrade, "A survey on big data for trajectory analytics," *ISPRS Int. J. Geo-Inf.*, vol. 9, no. 2, p. 88, 2020, doi: 10.3390/ijgi9020088.

[21] C. Parent, S. Spaccapietra, C. Renso, G. Andrienko, N. Andrienko, V. Bogorny, M. L. Damiani, A. Gkoulalas-Divanis, J. Macedo, N. Pelekis, Y. Theodoridis, and Z. Yan, "Semantic trajectories modeling and analysis," *ACM Comput. Surveys*, vol. 45, no. 4, pp. 1–32, Aug. 2013, doi: 10.1145/2501654.2501656.

[22] X. Kong et al., "Big trajectory data: A survey of applications and services," *IEEE Access*, vol. 6, pp. 58295–58306, 2018, doi: 10.1109/ACCESS.2018.2873779.

[23] J. Bian, D. Tian, Y. Tang, and D. Tao, "A survey on trajectory clustering analysis," 2018, *arXiv:1802.06971*.

[24] R. Xu and D. C. Wunsch, "Survey of clustering algorithms," *IEEE Trans. Neural Netw.*, vol. 16, no. 3, pp. 645–678, Nov. 2005.

[25] S. Gaffney, "Trajectory clustering with mixtures of regression models," in *Proc. 5th ACM SIGKDD Int. Conf. Knowl. Discovery Data Mining*, 2013, pp. 63–72, doi: 10.1145/312129.312198.

[26] J. Alon, S. Sclaroff, G. Kollios, and V. Pavlovic, "Discovering clusters in motion time-series data," in *Proc. IEEE Comput. Soc. Conf. Comput. Vis. Pattern Recognit.*, 2003, p. I, doi: 10.1109/CVPR.2003.1211378.

[27] O. Maimon and L. Rokach, *Data Mining and Knowledge Discovery Handbook*, vol. 14. New York, NY, USA: Springer, 2010.

[28] M. Ankerst, M. M. Breunig, H.-P. Kriegel, and J. Sander, "OPTICS: Ordering points to identify the clustering structure," *ACM SIGMOD Rec.*, vol. 28, no. 2, pp. 49–60, Jun. 1999.

[29] M. Daszykowski and B. Walczak, "Density-based clustering methods," in *Comprehensive Chemometrics*. Amsterdam, The Netherlands: Elsevier, 2009, doi: 10.1016/B978-044452701-1.00067-3.

[30] M. Nanni and D. Pedreschi, "Time-focused clustering of trajectories of moving objects," *J. Intell. Inf. Syst.*, vol. 27, no. 3, pp. 267–289, 2006.

[31] D. Birant and A. Kut, "ST-DBSCAN: An algorithm for clustering spatial–temporal data," *Data Knowl. Eng.*, vol. 60, no. 1, pp. 208–221, Jan. 2007, doi: 10.1016/j.datak.2006.01.013.

[32] S. J. Gaffney, A. W. Robertson, P. Smyth, S. J. Camargo, and M. Ghil, "Probabilistic clustering of extratropical cyclones using regression mixture models," *Climate Dyn.*, vol. 29, no. 4, pp. 423–440, Jun. 2007.

[33] J. Lee and J. Han, "Trajectory clustering: A partition-and-group framework?" in *Proc. Int. Conf. Manag. Data*, 2007, pp. 593–604.

[34] F. Schwenker and E. Trentin, "Pattern classification and clustering: A review of partially supervised learning approaches," *Pattern Recognit. Lett.*, vol. 37, pp. 4–14, Feb. 2014, doi: 10.1016/j.patrec.2013.10.017.

[35] S. B. Kotsiantis, I. D. Zaharakis, and P. E. Pintelas, "Machine learning: A review of classification and combining techniques," *Artif. Intell. Rev.*, vol. 26, no. 3, pp. 159–190, Nov. 2006, doi: 10.1007/s10462-007-9052-3.

[36] A. Bolbol, T. Cheng, I. Tsapakis, and J. Haworth, "Inferring hybrid transportation modes from sparse GPS data using a moving window SVM classification," *Comput., Environ. Urban Syst.*, vol. 36, no. 6, pp. 526–537, Nov. 2012, doi: 10.1016/j.compenvurbsys.2012.06.001.

[37] Y. Zheng, Y. Chen, Q. Li, X. Xie, and W.-Y. Ma, "Understanding transportation modes based on GPS data for Web applications," *ACM Trans. Web*, vol. 4, no. 1, pp. 1–36, Jan. 2010, doi: 10.1145/1658373.1658374.
[38] D. Patel, C. Sheng, W. Hsu, and M. L. Lee, "Incorporating duration information for trajectory classification," in *Proc. IEEE 28th Int. Conf. Data Eng.*, Apr. 2012, pp. 1132–1143, doi: 10.1109/ICDE.2012.72.
[39] J.-Y. Chemin, "About weak-strong uniqueness for the 3D incompressible Navier-Stokes system," *Commun. Pure Appl. Math.*, vol. 64, no. 12, pp. 1587–1598, Dec. 2011, doi: 10.1002/cpa.20386.
[40] J. D. Mazimpaka and S. Timpf, "Trajectory data mining: A review of methods and applications," *J. Spatial Inf. Sci.*, vol. 13, pp. 61–99, Dec. 2016, doi: 10.5311/josis.2016.13.263.
[41] S. Nasreen, M. A. Azam, K. Shehzad, U. Naeem, and M. A. Ghazanfar, "Frequent pattern mining algorithms for finding associated frequent patterns for data streams: A survey," *Proc. Comput. Sci.*, vol. 37, pp. 109–116, Sep. 2014, doi: 10.1016/j.procs.2014.08.019.
[42] M. Wachowicz, R. Ong, C. Renso, and M. Nanni, "Finding moving flock patterns among pedestrians through collective coherence," *Int. J. Geographical Inf. Sci.*, vol. 25, no. 11, pp. 1849–1864, Nov. 2011, doi: 10.1080/13658816.2011.561209.
[43] H. Jeung, M. L. Yiu, X. Zhou, C. S. Jensen, and H. T. Shen, "Discovery of convoys in trajectory databases," *Proc. PVLDB*, vol. 1, no. 1, pp. 1068–1080, 2008, doi: 10.14778/1453856.1453971.
[44] Z. Li, B. Ding, J. Han, and R. Kays, "Swarm: Mining relaxed temporal moving object clusters," *Proc. VLDB Endowment*, vol. 3, no. 1, pp. 723–734, 2010, doi: 10.14778/1920841.1920934.
[45] S. Sidiropoulos, A. Majumdar, K. Han, and W. Ochieng, "Identifying significant traffic flow patterns in multi-airport systems terminal manoeuvring areas under uncertainty," in *Proc. 16th AIAA Aviation Technol., Integr., Oper. Conf.*, Jun. 2016, pp. 1–19, doi: 10.2514/6.2016-3162.
[46] G. Antonini and J. P. Thiran, "Counting pedestrians in video sequences using trajectory clustering," *IEEE Trans. Circuits Syst. Video Technol.*, vol. 16, no. 8, pp. 1008–1020, Aug. 2016.
[47] X. Olive and L. Basora, "Detection and identification of significant events in historical aircraft trajectory data," *Transp. Res. C, Emerg. Technol.*, vol. 119, Oct. 2020, Art. no. 102737, doi: 10.1016/j.trc.2020.102737.
[48] X. Olive and L. Basora, "Deep trajectory clustering with autoencoders," in *Proc. 9th Int. Conf. Res. Air Transp.*, 2020, pp. 1–8.
[49] M. A. A. Carmona, F. S. Nieto, and C. E. V. Gallego, "A data-driven methodology for characterization of a terminal manoeuvring area in multi-airport systems," *Transp. Res. C, Emerg. Technol.*, vol. 111, pp. 185–209, Feb. 2020, doi: 10.1016/j.trc.2019.12.011.
[50] M. C. R. Murça, R. J. Hansman, L. Li, and P. Ren, "Flight trajectory data analytics for characterization of air traffic flows: A comparative analysis of terminal area operations between New York, Hong Kong and Sao Paulo," *Transp. Res. C, Emerg. Technol.*, vol. 97, pp. 324–347, Dec. 2018, doi: 10.1016/j.trc.2018.10.021.
[51] A. Bombelli, L. Soler, E. Trumbauer, and K. D. Mease, "Strategic air traffic planning with Fréchet distance aggregation and rerouting," *J. Guid., Control, Dyn.*, vol. 40, no. 5, pp. 1117–1129, May 2017, doi: 10.2514/1.G002308.
[52] H. Arneson, A. Bombelli, A. Segarra-Torne, and E. Tse, "Analysis of convective-weather impact on pre-departure routing decisions for flights traveling between Fort Worth Center and New York Air Center," in *Proc. AIAA*, Jun. 2017, pp. 1-12, doi: 10.2514/6.2017-3593.
[53] P. Ren and L. Li, "Characterizing air traffic networks via large-scale aircraft tracking data: A comparison between China and the U.S. Networks," *J. Air Transp. Manage.*, vol. 67, pp. 181–196, Mar. 2018, doi: 10.1016/j.jairtraman.2017.12.005.
[54] Y. Liu, M. Hansen, M. O. Ball, D. J. Lovell, C. Chuang, and J. M. Gulding, "Causal analysis of en route flight inefficiency—The U.S. experience," in *Proc. 12th USA/Eur. Air Traffic Manag.*, 2017, pp. 27–30.
[55] E. Schubert, J. Sander, M. Ester, H. P. Kriegel, and X. Xu, "DBSCAN revisited, revisited: Why and how you should (Still) use DBSCAN," *ACM Trans. Database Syst.*, vol. 42, no. 3, pp. 1–21, Sep. 2017, doi: 10.1145/3068335.
[56] A. M. Fahim, A. M. Salem, F. A. Torkey, and M. A. Ramadan, "An efficient enhanced k-means clustering algorithm," *J. Zhejiang Univ.-SCIENCE A*, vol. 7, no. 10, pp. 1626–1633, Oct. 2006, doi: 10.1631/jzus.2006.A1626.
[57] S. J. Corrado, T. G. Puranik, O. J. Pinon, and D. N. Mavris, "Trajectory clustering within the terminal airspace utilizing a weighted distance function," *Multidisciplinary Digit. Publishing Inst. Proc.*, vol. 59, no. 1, p. 7, 2020, doi: 10.3390/proceedings2020059007.
[58] M. C. R. Murça and R. J. Hansman, "Data-driven modeling of air traffic flows for advanced air traffic management," Ph.D. thesis, Massachusetts Inst. Technol., Cambridge, MA, USA, 2018.
[59] L. Basora, J. Morio, and C. Mailhot, "A trajectory clustering framework to analyse air traffic flows," in *Proc. 7th SESAR Innov. Days*, Nov. 2017, pp. 1–8.
[60] X. Olive and J. Morio, "Trajectory clustering of air traffic flows around airports," *Aerosp. Sci. Technol.*, vol. 84, pp. 776–781, Jan. 2019, doi: 10.1016/j.ast.2018.11.031.
[61] J. Rios, J. Homola, N. Craven, P. Verma, and V. Baskaran, "Strategic deconfliction performance (results and analysis from the NASA UTM technical capability level 4 demonstration)," NASA, Washington, DC, USA, 2020.
[62] (2020). *CORUS Project U-Space Concept of Operations (U-Space ConOps)*. [Online]. Available: https://www.eurocontrol.int/project/concept-operations-european-utm-systems
[63] P. Kopardekar, J. Rios, T. Prevot, M. Johnson, J. Jung, and J. E. Robinson, "Unmanned aircraft system traffic management (UTM) concept of operations," in *Proc. 16th AIAA Aviat. Technol. Integr. Oper. Conf.*, 2016, pp. 1–16.
[64] C. Yan, L. Fu, J. Zhang, and J. Wang, "A comprehensive survey on UAV communication channel modeling," *IEEE Access*, vol. 7, pp. 107769–107792, 2019, doi: 10.1109/ACCESS.2019.2933173.
[65] A. A. Saadi, A. Soukane, Y. Meraihi, A. B. Gabis, S. Mirjalili, and A. Ramdane-Cherif, *UAV Path Planning Using Optimization Approaches: A Survey*, vol. 29, no. 6. Cham, Switzerland: Springer, 2022.
[66] S. Aggarwal and N. Kumar, "Path planning techniques for unmanned aerial vehicles: A review, solutions, and challenges," *Comput. Commun.*, vol. 149, pp. 270–299, Jan. 2020, doi: 10.1016/j.comcom.2019.10.014.
[67] T. Cabreira, L. Brisolara, and P. R. Ferreira, Jr., "Survey on coverage path planning with unmanned aerial vehicles," *Drones*, vol. 3, no. 1, p. 4, Jan. 2019, doi: 10.3390/drones3010004.
[68] A. Al-Kaff, D. Martín, F. García, A. de la Escalera, and J. M. Armingol, "Survey of computer vision algorithms and applications for unmanned aerial vehicles," *Expert Syst. Appl.*, vol. 92, pp. 447–463, Feb. 2018, doi: 10.1016/j.eswa.2017.09.033.
[69] L. M. Belmonte, R. Morales, and A. Fernández-Caballero, "Computer vision in autonomous unmanned aerial vehicles—A systematic mapping study," *Appl. Sci.*, vol. 9, no. 15, pp. 1–34, 2019, doi: 10.3390/app9153196.
[70] J. Moon, S. Papaioannou, C. Laoudias, P. Kolios, and S. Kim, "Deep reinforcement learning multi-UAV trajectory control for target tracking," *IEEE Internet Things J.*, vol. 8, no. 20, pp. 15441–15455, Oct. 2021.
[71] D. Wang, D. Tan, and L. Liu, "Particle swarm optimization algorithm: An overview," *Soft Comput.*, vol. 22, no. 2, pp. 387–408, 2018, doi: 10.1007/s00500-016-2474-6.
[72] H. P. Dai, D. D. Chen, and Z. S. Zheng, "Effects of random values for particle swarm optimization algorithm," *Algorithms*, vol. 11, no. 2, pp. 1–20, 2018, doi: 10.3390/A11020023.
[73] A. P. Soares, "Exploring the range of weather impacts on uas operations," *J. Chem. Inf. Model.*, vol. 53, no. 9, pp. 1689–1699, 2013.
[74] E. Capello, G. Guglieri, and F. Quagliotti, "A waypoint-based guidance algorithm for mini UAVs," *IFAC Proc. Volumes*, vol. 46, no. 37, pp. 120–125, 2013.
[75] A. Alharbi, A. Poujade, K. Malandrakis, I. Petrunin, D. Panagiotakopoulos, and A. Tsourdos, "Rule-based conflict management for unmanned traffic management scenarios," in *Proc. AIAA/IEEE 39th Digit. Avionics Syst. Conf. (DASC)*, 2020, pp. 1–10, doi: 10.1109/DASC50938.2020.9256690.
[76] M. C. R. Murça and R. J. Hansman, "Identification, characterization, and prediction of traffic flow patterns in multi-airport systems," *IEEE Trans. Intell. Transp. Syst.*, vol. 20, no. 5, pp. 1683–1696, May 2019, doi: 10.1109/TITS.2018.2833452.
[77] K. Dorling, J. Heinrichs, G. G. Messier, and S. Magierowski, "Vehicle routing problems for drone delivery," *IEEE Trans. Syst., Man, Cybern., Syst.*, vol. 47, no. 1, pp. 70–85, Jan. 2017, doi: 10.1109/TSMC.2016.2582745.
[78] M. Erdelj and E. Natalizio, "UAV-assisted disaster management: Applications and open issues," in *Proc. Int. Conf. Comput., Netw. Commun. (ICNC)*, 2016, pp. 1–5, doi: 10.1109/ICCNC.2016.7440563.
[79] G. Radzki, P. Golinska-Dawson, G. Bocewicz, and Z. Banaszak, "Modelling robust delivery scenarios for a fleet of unmanned aerial vehicles in disaster relief missions," *J. Intell. Robot. Syst.*, vol. 103, no. 4, pp. 1–18, 2021, doi: 10.1007/s10846-021-01502-2.
[80] T. Larrabee, H. Chao, M. Rhudy, Y. Gu, and M. R. Napolitano, "Wind field estimation in UAV formation flight," in *Proc. Amer. Control Conf.*, Jun. 2014, pp. 5408–5413, doi: 10.1109/ACC.2014.6859266.
[81] M. Besiou, A. J. Pedraza-Martinez, and L. N. Van Wassenhove, "OR applied to humanitarian operations," *Eur. J. Oper. Res.*, vol. 269, no. 2, pp. 397–405, Sep. 2018, doi: 10.1016/j.ejor.2018.02.046.

[82] M. C. R. Murça, M. X. Guterres, M. de Oliveira, J. B. Tarelho Szenczuk, and W. S. S. Souza, "Characterizing the Brazilian airspace structure and air traffic performance via trajectory data analytics," *J. Air Transp. Manage.*, vol. 85, Jun. 2020, Art. no. 101798, doi: 10.1016/j.jairtraman.2020.101798.
[83] M. Peng and W. Meng, "Cooperative obstacle avoidance for multiple UAVs using spline_VO method," *Sensors*, vol. 22, no. 5, p. 1947, Mar. 2022, doi: 10.3390/s22051947.
[84] G. Gramajo and P. Shankar, "An efficient energy constraint based UAV path planning for search and coverage," *Int. J. Aerosp. Eng.*, vol. 2017, pp. 1–13, Dec. 2017, doi: 10.1155/2017/8085623.
[85] M. Lalak and D. Wierzbicki, "Methodology of detection and classification of selected aviation obstacles based on UAV dense image matching," *IEEE J. Sel. Topics Appl. Earth Observ. Remote Sens.*, vol. 15, pp. 1869–1883, 2022, doi: 10.1109/JSTARS.2022.3149105.
[86] K. J. Hall, "Algorithms and programs for the rapid computation of area and center of mass," *Comput. Geosci.*, vol. 1, no. 3, pp. 203–205, 1976.
[87] B. Hilburn, "Cognitive complexity in air traffic control: A literature review," Eurocontrol, Brussels, Belgium, Tech. Rep. 04/04, 2004.
[88] A. Elgammal, R. Duraiswami, D. Harwood, and L. S. Davis, "Background and foreground modeling using nonparametric kernel density estimation for visual surveillance," *Proc. IEEE*, vol. 90, no. 7, pp. 1151–1162, 2002, doi: 10.1109/JPROC.2002.801448.
[89] M. Smith, M. Goodchild, and P. Longley, *Geospatial Analysis, a Comprehensive Guide to Principles, Techniques and Software Tools*, 6th ed. Winchelsea, U.K.: The Winchelsea Press, 2019.
[90] T. Ahola, K. Virrantaus, J. M. Krisp, and G. J. Hunter, "A spatio-temporal population model to support risk assessment and damage analysis for decision-making," *Int. J. Geographical Inf. Sci.*, vol. 21, no. 8, pp. 935–953, Sep. 2007, doi: 10.1080/13658810701349078.
[91] R. Laxhammar, G. Falkman, and E. Sviestins, "Anomaly detection in sea traffic—A comparison of the Gaussian mixture model and the kernel density estimator," in *Proc. 12th Int. Conf. Inf. Fusion*, Feb. 2009, pp. 756–763.
[92] B. W. Silverman, *Density Estimation for Statistics and Data Analysis*, 1st ed. Evanston, IL, USA: Routledge, 1998, doi: 10.1201/9781315140919.

ABDULRAHMAN ALHARBI received the B.S. degree in computer science from King Saud University, Saudi Arabia, in 2004, and the M.S. degree in computer science from Huddersfield University, U.K., in 2012. He is currently pursuing the Ph.D. degree in data analytics with the School of Aerospace, Transport and Manufacturing (SATM), Cranfield University. He has been working as an IT Officer with the Royal Saudi Air Force (RSAF), since 2005. His research interests include the use of data analytics and machine learning for air traffic management diagnostics and optimization, with a focus on UTM operations.

IVAN PETRUNIN (Member, IEEE) received the M.Sc. degree in design of electronic equipment from the National Technical University of Ukraine, in 1998, and the Ph.D. degree in vibroacoustic damage detection from Cranfield University, in 2012. He is currently a Senior Lecturer in signal processing for autonomous systems with the Centre for Autonomous and Cyber-Physical Systems, School of Aerospace, Transport and Manufacturing, Cranfield University. His expertise covers areas of signal processing and artificial intelligence with application to cognitive communication, resilient navigation and timing, radar systems, non-destructive testing, material characterization, and condition monitoring of rotating machinery. In these areas, he has published over 90 journals and conference papers. He is a member of the IEEE Signal Processing Society, the Royal Institute of Navigation, and an Elected Member of the British Institute of Non-Destructive Testing.

DIMITRIOS PANAGIOTAKOPOULOS received the M.Eng. degree in electrical and electronic engineering from the University of Hull, in 2004, and the Ph.D. degree in satellite navigation and positioning systems from Imperial College London, in 2009. He is currently the Head of the Advanced Air Mobility (AAM) Research Group, Centre for Autonomous and Cyber-Physical Systems, School of Aerospace, Transport and Manufacturing, Cranfield University. With over 15 years industrial experience in air traffic management, enabling the path towards its digitalization towards increased automation and autonomy, he currently focuses the development of technologies, services and regulatory framework required to fully unlock the potential of autonomous, and uncrewed systems for the airborne movement of people and goods.

2022-12-12

Modeling and characterization of traffic flow patterns and identification of airspace density for UTM application

Alharbi, Abdulrahman

IEEE

Alharbi A, Petrunin I, Panagiotakopoulos D. (2022) Modeling and characterization of traffic flow patterns and identification of airspace density for UTM application. IEEE Access, Volume 10, pp. 130110-130134

https://doi.org/10.1109/ACCESS.2022.3228828